Redox Biology 64 (2023) 102786

Contents lists available at ScienceDirect

Redox Biology

journal homepage: www.elsevier.com/locate/redox

Metformin inhibits methylglyoxal-induced retinal pigment epithelial cell death and retinopathy via AMPK-dependent mechanisms: Reversing mitochondrial dysfunction and upregulating glyoxalase 1

Ponarulselvam Sekar [a,b], George Hsiao [b], Shu-Hao Hsu [c], Duen-Yi Huang [a], Wan-Wan Lin [a,b,d,*], Chi-Ming Chan [e,f,**]

[a] Department of Pharmacology, College of Medicine, National Taiwan University, Taipei, Taiwan
[b] Graduate Institute of Medical Sciences, Taipei Medical University, Taipei, Taiwan
[c] Medical Research Center, Cardinal Tien Hospital, New Taipei City, Taiwan
[d] Department and Graduate Institute of Pharmacology, National Defense Medical Center, Taipei, Taiwan
[e] Department of Ophthalmology, Cardinal Tien Hospital, New Taipei City, Taiwan
[f] School of Medicine, Fu Jen Catholic University, New Taipei City, Taiwan

ARTICLE INFO

Keywords:
Diabetic retinopathy
Methylglyoxal
Metformin
AMPK
Mitochondria
Glyoxalase 1
Retinal pigment epithelial cells

ABSTRACT

Diabetic retinopathy (DR) is a major cause of blindness in adult, and the accumulation of advanced glycation end products (AGEs) is a major pathologic event in DR. Methylglyoxal (MGO), a highly reactive dicarbonyl compound, is a precursor of AGEs. Although the therapeutic potential of metformin for retinopathy disorders has recently been elucidated, possibly through AMPK activation, it remains unknown how metformin directly affects the MGO-induced stress response in retinal pigment epithelial cells. Therefore, in this study, we compared the effects of metformin and the AMPK activator A769662 on MGO-induced DR in mice, as well as evaluated cytotoxicity, mitochondrial dynamic changes and dysfunction in ARPE-19 cells. We found MGO can induce mitochondrial ROS production and mitochondrial membrane potential loss, but reduce cytosolic ROS level in ARPE-19 cells. Although these effects of MGO can be reversed by both metformin and A769662, we demonstrated that reduction of mitochondrial ROS production rather than restoration of cytosolic ROS level contributes to cell protective effects of metformin and A769662. Moreover, MGO inhibits AMPK activity, reduces LC3II accumulation, and suppresses protein and gene expressions of MFN1, PGC-1α and TFAM, leading to mitochondrial fission, inhibition of mitochondrial biogenesis and autophagy. In contrast, these events of MGO were reversed by metformin in an AMPK-dependent manner as evidenced by the effects of compound C and AMPK silencing. In addition, we observed an AMPK-dependent upregulation of glyoxalase 1, a ubiquitous cellular enzyme that participates in the detoxification of MGO. In intravitreal drug-treated mice, we found that AMPK activators can reverse the MGO-induced cotton wool spots, macular edema and retinal damage. Functional, histological and optical coherence tomography analysis support the protective actions of both agents against MGO-elicited retinal damage. Metformin and A769662 via AMPK activation exert a strong protection against MGO-induced retinal pigment epithelial cell death and retinopathy. Therefore, metformin and AMPK activator can be therapeutic agents for DR.

1. Introduction

In the center of the retina, macula provides central vision and is the most important part of the eye. The retinal pigment epithelium (RPE) is a monolayer located between photoreceptor cells and Bruch's membrane, and orchestrates the outer blood-retinal barrier. The RPE carries out several important functions for the maintenance of the visual system, such as transmitting information, transferring nutrients to the photoreceptors, and phagocytosing metabolic waste. Thus, structural injury and dysfunction of the RPE underlie many inherited and acquired

* Corresponding author. Department of Pharmacology, College of Medicine, National Taiwan University, Taipei, Taiwan.
** Corresponding author. Department of Ophthalmology, Cardinal Tien Hospital, New Taipei City, Taiwan.
E-mail addresses: wwllaura1119@ntu.edu.tw (W.-W. Lin), m212092001@tmu.edu.tw (C.-M. Chan).

https://doi.org/10.1016/j.redox.2023.102786
Received 21 February 2023; Received in revised form 9 June 2023; Accepted 14 June 2023
Available online 15 June 2023

retinal diseases [1,2].

Diabetic retinopathy (DR) is a common complication of diabetes mellitus (DM) and is one of the major vascular complication in diabetic patients worldwide. Hyperglycemia, which gives rise to accumulation of advanced glycation end products (AGEs), is the primary factor in the development of DR [3]. The primary formation of AGEs is majorly from non-enzymatic reaction of glucose, and the reactive carbonyl metabolites of glucose exert irreversibly covalent binding to DNA, proteins and lipids [4]. The resulting dicarbonyl stress increases the accumulation of AGEs, leading to damage of various tissues including retina in diabetic patients and aged peoples [5]. Methylglyoxal (MGO) is a highly reactive dicarbonyl compound and a natural product of glycolysis present under normal physiological conditions in all biological systems [6]. Increased glycolytic flux combined with oxidative stress can increase the generation of MGO, particularly in diabetes. Plasma levels of MGO are higher in patients with diabetes (4–400 μM) than in healthy controls (approximately 0.5 μM), and might contribute to the pathogenesis of diabetes-related vascular diseases, including DR [7,8]. To date, multifaceted actions of MGO have been demonstrated in inducing stress responses and contributing to cell death [9–11]. These include modification of proteins by non-enzymatic glycation and oxidation reactions [10], irreversible effects on protein misfolding [12], induction of autophagy flux [13], activation of matrix metalloproteinases [14] and dysfunction of SERCA pump [15]. In our previous study, we found that MGO can induce retinal pigment epithelial ARPE-19 cell death through a reactive oxygen species (ROS)-dependent manner, involving mitochondrial membrane potential (MMP) loss and intracellular calcium increases [16].

To date the therapy for DR is still an emerging issue. Besides improving glycemia control and reducing oxidative stress, an effective way to attenuate dicarbonyl stress-mediated RPE damage in DM patients remains an elusive goal. Recently, clinical data have indicated that metformin, the first-line anti-diabetic agent, may be a new therapeutic strategy for retinal diseases, including age-related macular degeneration (AMD) [17–21]. Newly discovered functions of metformin in animal and cell studies also support its potential use in AMD [22]. In hyperglycemia mouse model, metformin can alleviate retinal vasculature [23] and reduce retinal cell death [14,24]. In vital dye-induced damage of RPE and in retinitis pigmentosa mice model, metformin has been shown to provide protection [25–27]. In cell studies, metformin has demonstrated the ability to protect photoreceptors and RPE cells from acute injury and delay inherited retinal degeneration. Taken together, although metformin has therapeutic potential in DR, it remains unclear whether this benefit results from the direct action of metformin in the retina, beyond its hypoglycemia effect.

Several studies have demonstrated the underlying mechanisms for the protective action of metformin in various cell types. The protection is associated with decreased oxidative stress [28,29], increased mitochondrial energy production [30] and autophagy [26], as well as reduced VEGF-A expression [24,31]. Nevertheless, metformin may also directly suppress respiratory complex I, leading to deteriorate mitochondrial dysfunction and in turn activate AMP-activated protein kinase (AMPK) [32]. However, the precise effects of metformin in most cell models regarding this action are not well understood. Interestingly, our recent work demonstrates that compartmental ROS might have bifurcated actions in RPE cell viability. Cytosolic ROS-mediated autophagy and subsequent mitochondrial dynamic balance can counteract the cell death pathways induced by oxidative toxic agent sodium iodate in RPE cells [33]. Altogether, the direct effect of metformin in MGO-stressed RPE cells and the detailed underling mechanisms that relate to AMPK, cellular and mitochondrial ROS, mitochondrial dynamics, oxidative phosphorylation and autophagy remain unclear up to now. Therefore, in this study, we compared the actions of metformin and the specific AMPK activator A769662 to elucidate whether both agents can reduce MGO-induced retinopathy in mice and alleviate cell dysfunction in ARPE-19 cells.

2. Materials and methods

2.1. Reagents

MGO (M0252), *N*-acetyl cysteine (NAC) (A7250), 3-methyladenine (3-MA) (M9281), DCFDA (dichlorofluorescein diacetate) (SKU 287810), DHE (dihydroethidium) (D7008), oligomycin (75351), FCCP (carbonyl cyanide-*p*-trifluoromethoxyphenylhydrazone) (C2920), rotenone (R8875), antimycin A (A8674), compound C (SKU 171260), BBGC (*S*-*p*-bromobenzylglutathione cyclopentyl diester) (SML 1306) and JC-1 (T4069) were obtained from Sigma-Aldrich Co (St Louis, MO, USA). Metformin (HY-17471 A) was purchased from MedChemexpress (Monmouth Junction, NJ, USA). A769662 (336) and MitoPY1 (4428) were obtained from Tocris Biosciences (Bristol, UK). Antibodies specific for dynamin-related protein (DRP)-1 (8570), PGC-1α (2178s), phospho-AMPK (T172) (SAB4503754), AMPKα (2532s), cleaved caspase 3 (9661s), Bax (2772s), Bcl-2 (2876s) and Tom 20 (42406s) were purchased from Cell Signaling Technology (Beverly, MA, USA). Antibodies specific for mitofusin 1 (MFN1) (ab191853), mitofusin 2 (MFN2) (ab124773) and optic atrophy 1 (OPA1) (ab42364) were purchased from Abcam (Cambridge, UK). The β-actin (sc-47778) antibody was purchased from Santa Cruz Biotechnology (Santa Cruz, CA, USA). Mitotracker green (M7514) and MitoSOX (M36008) were purchased from Thermo Fischer Scientific (Waltham, MA, USA). Dulbecco's Modified Eagle's Medium/Nutrient Mixture F-12 (DMEM/F12) (D8900), penicillin, streptomycin (15240062) and trypsin-EDTA (25200072) were from Invitrogen (Rockville, MD, USA). Glyoxalase (GLO) 1 (K591) and GLO2 (K460) colorimetric activity assay kits were purchased from BioVision (San Francisco, USA). ECL reagent (Western blotting lightning chemiluminescence reagent plus) was purchased from PerkinElmer (Wellesley, MA, USA).

2.2. Animals

Male C57BL/6 mice (8 weeks old) were purchased from Laboratory Animal Center, National Taiwan University (Taipei, Taiwan). All animals were bred under pathogen-free conditions with controlled temperature and 12 h dark/light cycles in the Laboratory Animal Center, National Taiwan University. Mice experiments were conducted in accordance with institute regulation after receiving approval from the Ethics Committee of the National Taiwan University College of Medicine (No. 20210290).

2.3. Intravitreal injection of MGO

Mice were anesthetized with an intraperitoneal injection of ketamine and xylazine. Total volume of 1 μl containing PBS or agents such as metformin (5 μg), A769662 (20 pmol) or MGO (1.5 nmol) was injected intravitreally together into the eye using a 33-gauge needle with 10 μl syringe (Hamilton Bonaduz AG, Bonaduz, Switzerland) through the temporal limbus of the eye. In every mouse, the right eye was injected with the indicated drug and the left eye with PBS. Based on the volume of mouse vitreous cavity of 4–5 μl, the concentration of MGO (1.5 nmol) in vitreous fluid was estimated around 300 μM, and the concentrations of metformin (5 μg) and A769662 (20 pmol) were about 7 mM and 4 μM, respectively.

2.4. Scotopic electroretinography (ERG) analysis

Scotopic ERGs were used to analyze the rod and cone photoreceptor responses to light as previously described [34,35]. ERG system was composed of a MP-36 4-channel amplifier and acquisition system (Biopac Systems, Inc., Pershore, UK) connected to a PS33-PLUS photic stimulator (Grass Technologies, Warwick, RI USA). Recordings were obtained using a 10 msec flash stimulus with an intensity of 16 (19.1 cd s/m^2). ERG a-wave amplitude was recorded from baseline to the

negative peak, and the b-wave amplitude was measured from the trough of the a-wave to the peak of the positive wave. The temporal properties of the ERG response were defined by the time-to-peak (implicit time) of the a- and b-waves, and were measured from stimulus onset to the peak of the a- and b-waves.

2.5. Spectral-domain optical coherence tomography (SD-OCT) imaging

SD-OCT was used to non-invasively acquire cross-sectional tomographic images of the retina. This approach allowed for the monitoring of inner retinal morphology in live experimental animals. The Micron III intraocular imaging system (Phoenix Research Labs, Pleasanton, CA), composed of an OCT engine and a scanning lens, was used as reported [34,35]. OCT imaging was performed immediately after the ERG recording, and the OCT image was imported into the InSight XL software (Phoenix Research Laboratories) to measure the total retinal thickness as well as the thickness of the different retinal layers.

2.6. Tissue homogenization

Mice were anesthetized using ketamine and xylazine mixture, enucleated immediately and removed the extraocular tissue. Each eye ball was transferred into a 2 ml Precellys homogenization tube containing five 2.8-mm ceramic beads (Bertin Technologies, Rockville, Maryland, USA) and transferred in 100 μl of homogenization buffer with 1 X protease inhibitor (Roche, Mannheim, Germany) and homogenized using a tissue homogenizer (Minilys®; Bertin Technologies, Rockville, Maryland, USA) at 2300 g for 30 s. The homogenized samples were centrifuged at 18,000 g for 5 min at 4 °C, and the resulting supernatants were incubated at 4 °C for 30 min. The samples were subsequently centrifuged at 12,000 g for 20 min at 4 °C and stored at −80 °C.

2.7. H&E staining

Surgical specimens of the whole retinal tissues were fixed with Davidson solution (glacial acetic acid, 95% alcohol, 10% formalin and double distilled water in a ratio of 4:12:5:15) and paraffin-embedded for H&E staining as previously described [35]. Sagittal sections (5 μm) were subjected to hematoxylin staining for 40 s followed by eosin staining for 30 s. Subsequently, the tissue sections were examined under a light microscope after being mounted with Permount mounting medium.

2.8. Cell culture

Adult human RPE cell line ARPE-19 was purchased from Food Industry Research and Development Institute (Hsinchu, Taiwan). These cells were maintained in DMEM/F12 supplemented with 10% fetal bovine serum (GibcoBRL, Invitrogen Life Technologies, Carlsbad, CA, USA), 100 units/ml penicillin and 100 μg/ml streptomycin (Sigma-Aldrich Co.). The cells were cultured in a humidified incubator at 37 °C and 5% CO_2. For most of the experiments, cells reaching a 90–95% of confluence were starved and synchronized in serum-free DMEM for 24 h before they were subjected to further analysis.

2.9. RNA interference

Human si-AMPKα1/2 (sc-45312) and scramble nonspecific siRNA (sc-44236) were purchased from Santa Cruz Biotechnology (Dallas, Texas, USA) and human si-GLO1 (s5825) was from Thermo Fischer Scientific (Waltham, US). ARPE-19 cells were transfected with 100 nM siRNA by DharmaFECT transfection reagents (Dharmacon Research, Lafayette, CO, USA) at 50% confluence following the manufacturers' protocol. After siRNA transfection for 48 h, cells were harvested after treatment with the indicated drugs.

2.10. Annexin V-FITC/propidium iodide staining

The cell surface exposure of phosphatidylserine and the plasma membrane impairment of cells were assessed using Annexin V-FITC/propidium iodide (PI) Apoptosis Detection Kit (BioLegend, San Diego, CA, USA). Briefly, suspension of treated/control ARPE-19 cells, containing 5×10^5 cells, was washed with PBS and re-suspended in 0.5 ml cold binding buffer. Then, 1 μl of Annexin V-FITC and 2 μl of propidium iodide (PI) were added and the cells were incubated in the dark humidified incubator at 37 °C and 5% CO_2 for 30 min. Following incubation, the cells were centrifuged at 100×*g* for 5 min and the supernatant was removed. The cell pellet was re-suspended in 0.5 ml cold binding buffer, and 10 μl of the 30 μg/ml PI solution was added. Cell samples were placed on ice, away from light, and FITC and PI fluorescence were immediately measured by using flow cytometer (FACSCalibur, Franklin Lakes, NJ, USA). Data were analyzed using Cell Quest Pro software (Becton Dickinson, Franklin Lakes, NJ, USA). The populations of live cells, early apoptotic cells, late apoptotic and necrotic cells were determined.

2.11. Determination of the cytosolic and mitochondrial ROS

Cytosolic ROS production was detected using DCFDA for H_2O_2 and DHE for O_2^-, and mitochondrial ROS production was detected using mitoSOX and mitoPY1. After drug treatment, ARPE-19 cells were washed with PBS and incubated with 10 μM DCFDA, 5 μM DHE, 5 μM MitoSOX Red or 5 μM mitoPY1 at 37 °C for 30 min. Subsequently, the cells were washed in PBS and trypsinized, and then the fluorescence intensity was measured by flow cytometry (FACSCalibur, Franklin Lakes, NJ, USA) at excitation/emission wavelengths of 485/530 nm, 510/595 nm, 510/580 nm and 503/528 nm for DCFDA, DHE, mitoSOX and mitoPY1, respectively. For each sample, ROS production was expressed as mean fluorescence ratio (fluorescence of exposed cells/fluorescence of control cells) from the same experiment.

2.12. Measurement of mitochondrial oxygen consumption rate

The oxygen consumption rate (OCR) was measured by the extracellular flux analyzer Seahorse XF24 (Agilent technologies, CA, USA) as we previously described [36]. Cells were plated at 4×10^5 cells/well in a Seahorse 24-well V7 microplate and cultured in complete DMEM growth medium for 24 h in a 5% CO_2 incubator at 37 °C. Then, the medium was removed and the cells were incubated in XF assay medium in the absence of FBS for 1 h at 37 °C in measuring chamber without CO_2 input. The mitochondrial complex inhibitors such as oligomycin, FCCP, antimycin A1, and rotenone were freshly prepared in XF assay media, and their treated concentrations were 2.5 μM, 1 μM, 2.5 μM, and 2.5 μM, respectively. OCR was recorded as pMoles per minute. ATP turnover was measured after the treatment with oligomycin. Respiratory capacity was the maximum rate after the treatment of FCCP injection subtracted by the non-mitochondrial respiration.

2.13. Mitochondrial membrane potential measurement

To investigate the mitochondrial membrane potential, ARPE-19 cells were seeded in 6-well plates one day before the experiment. After treatment for indicated times, cells were incubated at 37 °C for 20 min with 5 μg/ml JC-1, then washed twice with PBS before subjecting to flow cytometry.

2.14. Mitochondrial imaging

Mitochondrial imaging was measured as previously described [36]. After stimulation, cells were fixed with 4% paraformaldehyde at 37 °C followed by permeabilization with 0.2% Triton X-100 for 15 min and blocking by 5% bovine serum albumin (BSA) in PBS and normal IgG

(1:300) for 1 h. For mitochondrial morphology, cells were treated with Tom20 antibody in 1% BSA overnight at 4 °C. After washing with sterilized PBS, cells were incubated with secondary antibody in 1% BSA (in PBS) for 1 h at room temperature and then mounted with DAPI Fluoromount-G (Cat. No. 0100–20, Southern Biotech, Birmingham, AL, USA). Images were processed using a 100 X Plan-Neofluar oil objective of LSM 880 in Airyscan SR microscopy (Carl Zeiss Micro Imaging GmbH, Jena, Germany).

2.15. Immunoblotting

After drug treatment, cells were harvested, sonicated and equal amounts of protein as determined by Bradford assay were subjected to SDS-PAGE and transferred using polyvinylidene difluoride membrane (PVDF). After incubation with 5% nonfat milk in tris buffered saline (TBST) (10 mM Tris, pH 8.0, 150 mM NaCl, 0.5% Tween 20) for 60 min, the membrane was washed thrice with TBST and incubated with selected antibodies at 4 °C for overnight. Membranes were washed thrice with TBST for 10 min and incubated with a horseradish peroxidase-conjugated anti-mouse or anti-rabbit antibodies (1:5000 dilution) for 2 h. Blots were then washed with TBST three times and detected with enhanced chemiluminescence detection reagent. Equal amounts of sample protein loading were standardized by using β-actin as the internal control.

2.16. Quantitative real-time PCR

Human mRNA expressions of PGC-1α, TFAM, MFN1, MFN2, OPA1, LC3, GLO1, and β-actin were determined by real-time PCR analysis. The specific primers for these gene expression were shown in Table 1. After the drug treatment, cells were harvested and homogenized with Tripure isolation reagents (Roche Applied Science, Indianapolis, IN, USA), and 1 μg of total RNA was reverse transcribed to cDNA with an RT-PCR kit (Promega, Heidelberg, Germany) according to the manufacturer's instructions. Real-time PCR was performed in 96-well plates with the fast start SYBR green master. PCR products were measured with an ABI Quant Studio 5 (Thermo Fischer Scientific, Waltham, Massachusetts, USA).

2.17. GLO1 and GLO2 activity assays

Enzymatic activity assays of GLO1 and GLO2 were determined using BioVision kits (#k591 for GLO1 and #k490 for GLO2). After drug treatment, cell lysates were prepared using ice-cold assay buffer containing protease inhibitors and kept on ice for 10 min. Samples were centrifuged at 13,200 g at 4 °C for 10 min. Supernatants were collected and kept on ice for the enzymatic assay as following the manufacturers' instructions.

Table 1
qPCR primers.

	Forward primer	Reverse primer
GLO-1	5-CTAGAGTTCTTGGAATGACGC-3	5-ATTGTGGTAACTCTGGGTCTCA-3
PGC1α	5-CCAAAGATGCGCTCTCGTTCA-3	5-CGGTGTCTGTAGTGGCTTGACT-3
TFAM	5-GTGGTTTTCATCTGTCTTGGCA-3	5-TTCCCTCCAACGCTGGGCAATT-3
MFN-1	5- GGTGAATGAGCGGCTTTCCAA-3	5- TCCTCCACCAAGAAATGCAGG-3
MFN-2	5- CCTGCTCTTCTCTCGATGCAA-3	5-TGTCTTCAAGGAAGGTGGCG-3
OPA-1	5-TGGCCTGGATAGCAGAAAGG-3	5-AGGATGTCCTTAATTGGGGTCG-3
LC3	5-GCGAGTTACCTCCCGCAG-3	5-GTACCTCCTTACAGCGGTCG-3
β-actin	5-CGGGGACCTGACTGACTACC-3	5-AGGAAGGCTGGAAGAGTGC-3

2.18. Statistical analysis

All data presented as mean ± standard error mean (S.E.M.) were obtained from at least three independent experiments. Multiple groups were compared by one-way analysis of variance and Bonferroni post-test, making use of Graph pad software (Graph Pad Software, San Diego, CA, USA). Two groups were compared with an unpaired Student's *t*-test and two-tail *p* value. Results were considered statistically significant when $p < 0.05$.

3. Results

3.1. Metformin inhibits MGO-induced cell death and reverses MGO-induced cytosolic ROS reduction in ARPE-19 cells

Previously, we and others found that MGO can induce ROS production, caspase 3 activation and cell apoptosis in ARPE-19 cells [16,37]. In this study, we determined the effects of metformin on cell viability and ROS levels. As expected, MGO (300 μg/ml) can induce time-dependent cell death within 16 h, with approximately 50% cell death observed after 6 h of incubation (Fig. 1A). Next, we set the MGO incubation time at 6 h and determined its concentration-dependency. Pretreating cells with metformin at 2, 6 or 20 mM for 30 min can attenuate MGO-induced cell death after 6 h incubation in a concentration-dependent manner (Fig. 1B). In addition, this cytoprotective action of metformin was still achieved when metformin was co-treated with MGO or post-treated after MGO exposure. When cell viability was determined after 6 h of MGO treatment, 2-h delay in administrating 6 mM metformin still resulted in a partial protection of the cells. When increasing metformin concentration to 20 mM, its cell protective effect was prolonged upon 4 h post-treatment (Fig. 1C). To correlate the cell protective action of metformin, we determined several apoptosis-related molecules. MGO (300 μg/ml) induced Bax expression and caspase-3 cleavage, but decreased Bcl-2 expression in ARPE-19 cells. All these cellular detrimental effects of MGO were prevented by 6 mM metformin (Fig. 1D). The quantification of Fig. 1D data was shown in the Supplementary Fig. 1.

To understand the protective mechanisms of metformin, we first determined the role of cellular ROS level by using DCFDA and DHE, specific probes for measuring intracellular H_2O_2 and O_2^- levels, respectively [38]. We found that MGO transiently increased cellular ROS which peaked at 60 min, and then time-dependently declined to 23% of control at 4 h. Although metformin (20 mM) itself had no effect on the cellular H_2O_2 production within 4 h incubation, it reversed the decreasing effect of MGO (Fig. 2A). This effect of metformin also displayed the concentration-dependency with complete reversal of cellular H_2O_2 level at 6 mM (Fig. 2B). Using DHE staining, similar to what we observed for cellular H_2O_2, the initially slight increase within 1 h and the gradual decrease of cellular O_2^- after MGO treatment were detected (Fig. 2C). Likewise, this effect was reversed by metformin in a concentration-dependent manner, with the complete abrogation at 20 mM metformin (Fig. 2D). These findings indicate that metformin can stabilize cellular ROS levels under basal resting condition and protect cells when exposed to MGO treatment.

3.2. Metformin reverses MGO-induced mitochondrial ROS production and mitochondrial membrane potential loss

Next, we determined the effect of metformin on mitochondrial ROS (mtROS) upon MGO stimulation. Using mitoSOX for measuring O_2^- in mitochondrial matrix, we found that MGO significantly increased mitochondrial O_2^-; however, its kinetic pattern was different from the changes of cellular ROS level measured by DCFDA and DHE. MGO-induced mitochondrial O_2^- increase was observed at 1 h, with a time-dependent increase for up to 8 h. Moreover, metformin (6 and 20 mM) attenuated this ROS increasing action of MGO (Fig. 3A). Besides

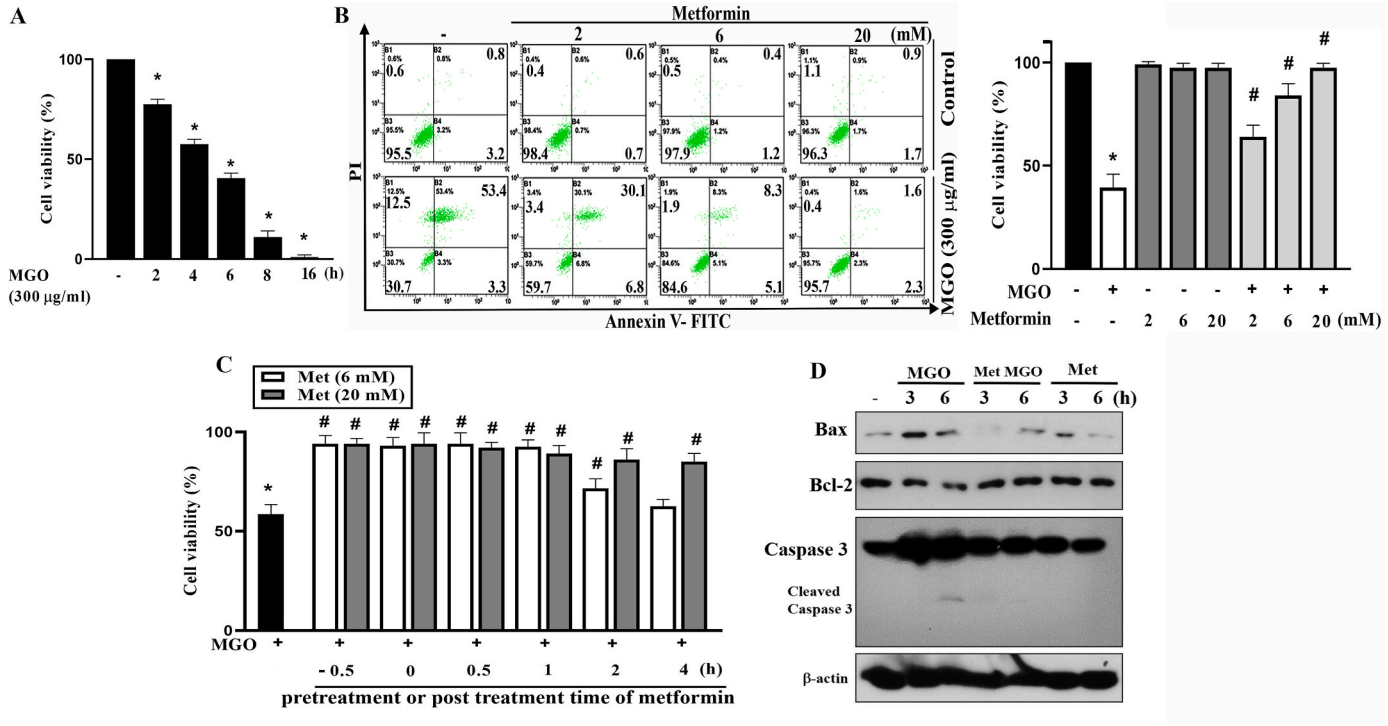

Fig. 1. Metformin protects RPE cells against MGO-induced cytotoxicity.
(A) ARPE-19 cells were stimulated with MGO (300 μg/ml) for indicated time points. Cell viability was determined by Annexin V-FITC/PI staining using FACScalibur. **(B)** Cells were pretreated with metformin (2, 6 and 20 mM) 30 min prior to MGO (300 μg/ml) treatment for 6 h. Cell viability was determined by Annexin V-FITC/PI staining. **(C)** Metformin (6 or 20 mM) was administered at 30 min pre-treatment before MGO, co-treatment with MGO, or post-treatment at 0.5, 1, 2, or 4 h after MGO (300 μg/ml). After 6 h of MGO treatment, cell viability was determined by Annexin V-FITC/PI staining. Data were the mean ± S.E.M. from at least 3 independent experiments. *p < 0.05, indicating the significant effect of MGO; #p < 0.05, indicating the blockade effect of metformin. **(D)** Cells were pretreated with 6 mM metformin for 30 min followed by MGO (300 μg/ml) treatment for 3 or 6 h. Cell lysates were prepared for immunoblotting. Data were representative of 3 independent experiments.

mitochondrial O_2^- we also used mitoPY1 to measure mitochondrial H_2O_2. As shown in Fig. 3B, MGO time-dependently increased mitochondrial H_2O_2 within 8 h and metformin (6 and 20 mM) inhibited this effect in a concentration-dependent manner. To further clarify the MGO-induced oxidative stress response in mitochondria, mitochondrial membrane potential (MMP) was measured. We found MGO decreased MMP and this response was simultaneously reversed by metformin in a concentration-dependent manner (Fig. 3C). Moreover, we measured the effect of metformin (6 mM) on mitochondrial OXPHOS after MGO treatment. After treating cells with metformin, we immediately placed the cells into apparatus for OCR measurement. We found MGO reduced resting OCR, ATP turnover and respiratory capacity, while metformin (6 mM) did not change these effects of MGO (Fig. 3D). From these findings, we suggest the cell protective effect of metformin may result from the inhibition of MGO-induced mitochondrial ROS production and MMP loss, but independent of oxidative phosphorylation suppression. In addition, the distinct changes of ROS levels as measured by DCFDA/DHE and mitoSOX/mitoPY1 upon MGO stimulation imply the existence of compartmental ROS changes. As cytosol is the major cellular component for DCFDA and DHE distribution [38], we suggest MGO can decrease cytosolic ROS production after 2–4 h incubation.

3.3. Reduction of mitochondrial ROS rather than restoration of cytosolic ROS contributes to the cell protective effect of metformin

The effects of MGO on decreasing cytosolic ROS level while concomitantly increasing mitochondrial ROS level are quite unique. Moreover, metformin can also concomitantly reverse both changes under MGO treatment. These observations raise our interest to further determine the role of cytosolic ROS in cell fate control. Another reason of this idea is we previously found that cellular ROS level is involved in autophagy induction which exerts a survival mechanism in ARPE-19 cells under a mitochondrial stress [33]. Therefore, we were interested in understanding the role of compartmental ROS in MGO-induced cell death. To this end, we used antioxidant *N*-acetylcysteine (NAC). We demonstrated that NAC (3, 10 mM) can concentration-dependently attenuate cell death caused by MGO in ARPE-19 cells, with complete protection at 10 mM. In the co-administration of metformin and NAC, complete cell protection was still observed (Fig. 4A). Next, we measured the effect of NAC on cytosolic ROS level. We found that NAC (10 mM) dramatically abolished cytosolic H_2O_2 production upon MGO with metformin incubation (Fig. 4B). As to cytosolic O_2^-, we also found similar effect of NAC to reduce cytosolic O_2^- level (Fig. 4C). Because both metformin and NAC can protect cells but exert different effects on cytosolic ROS, we suggest that cytosolic ROS level does not contribute to the protective actions of metformin and NAC. Another evidence for this suggestion is the observation that DPI , a cytosolic NADPH oxidase inhibitor did not have an impact on MGO-induced cytotoxicity or the cell-protective effect of metformin (Fig. 4D). To further elucidate the protective mechanisms of metformin and NAC, we determined mitochondrial O_2^- and H_2O_2. We found that NAC (3 mM) did not further reduce mtROS production under metformin + MGO treatment (Fig. 4E and F). These findings suggest that counteracting mitochondrial ROS production is the key for metformin and NAC to prevent cell death under MGO stress. In addition, we further determined the effect of NAC on OXPHOS after MGO treatment, similar to what we previously conducted for metformin. As shown in Fig. 4G, we found that NAC itself did not affect OCR. When co-treating with MGO, NAC reversed the inhibitory effects of MGO on resting OCR, ATP turnover and respiratory capacity.

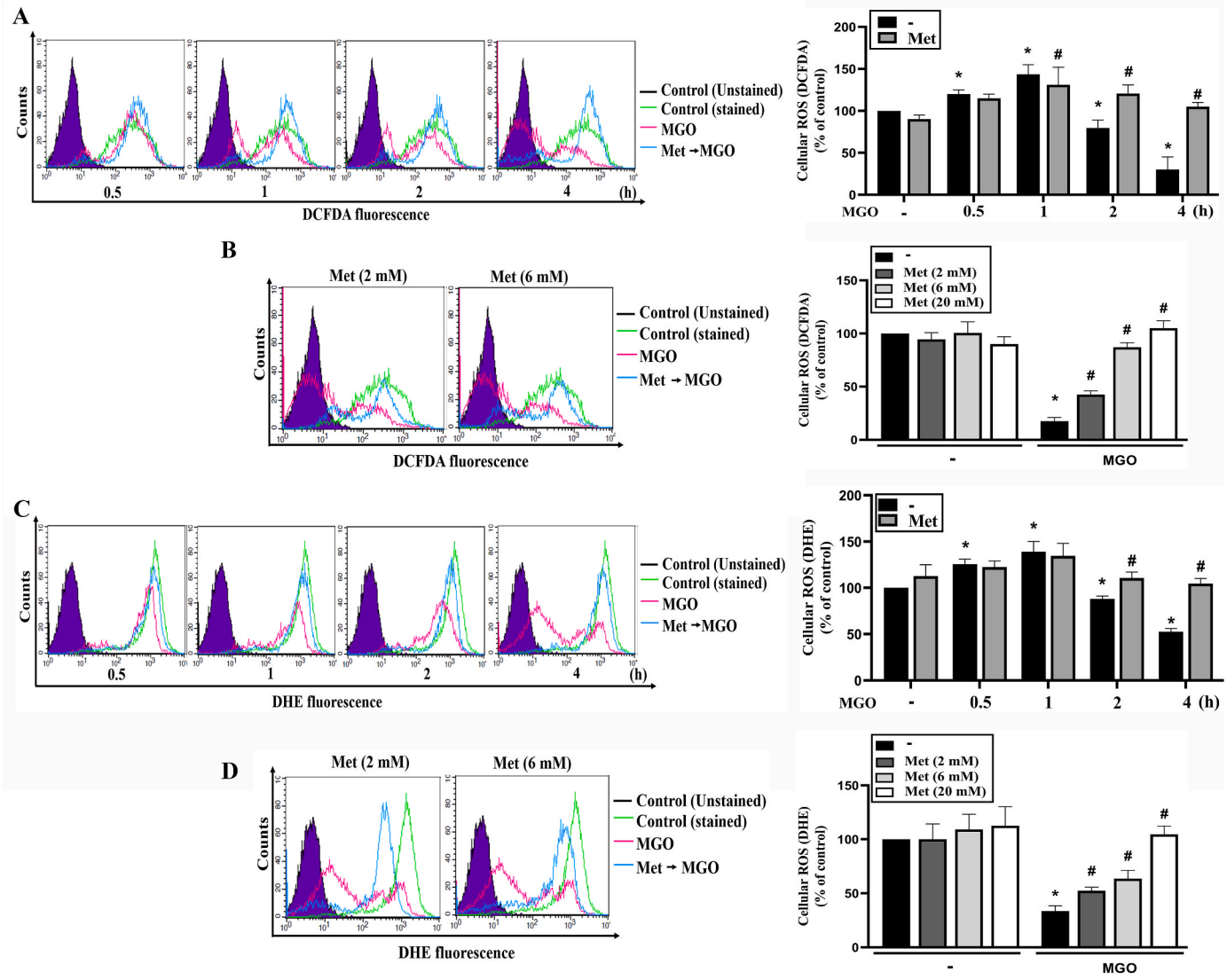

Fig. 2. Metformin can restore cellular ROS in MGO-stimulated cells.
(A, C) Cells were 30 min pretreated with metformin (6 mM) followed by MGO (300 μg/ml) treatment for 0.5, 1, 2 or 4 h. **(B, D)** Cells were pretreated with metformin (2, 6 or 20 mM) 30 min prior to MGO (300 μg/ml) incubation for 4 h. After treatment of MGO for indicated times, cellular ROS level was determined by using DCFDA **(A, B)** or DHE **(C, D)**. Data were the mean ± S.E.M. from at least 3 independent experiments. *$p < 0.05$, indicating the significant effect of MGO; #$p < 0.05$, indicating the significant reversal effect of metformin on MGO-induced cellular responses.

3.4. AMPK activation rather than complex I inhibition contributes to the protective effect of metformin

Because AMPK activation has been shown to exert antioxidant and mitochondrial regulation, we determined the role of AMPK in MGO-treated ARPE-19 cells. We found that MGO itself decreased AMPK activity, while metformin induced AMPK activation (Fig. 5A). We further explored the role of AMPK in regulating MGO-elicited stress events by using selective AMPK activator A769662. We found that, similar to metformin, A769662 (25 μM) activated AMPK (Fig. 5A) and protected cells against MGO-induced cytotoxicity (Fig. 5B). The quantification of Fig. 5A data was shown in the Supplementary Fig. 2. As with metformin, A769662 reversed the effects of MGO on ROS production, including the reduction of cytosolic H_2O_2 (Fig. 5C) and O_2^- (Fig. 5D), as well as the increases of mitochondrial O_2^- (Fig. 5E) and H_2O_2 (Fig. 5F). Furthermore, MGO-induced cytotoxicity was enhanced by AMPK inhibitor compound C and by AMPK silencing (Fig. 5G). Meanwhile, as the action of metformin, A769662 did not affect the inhibitory effects of MGO on resting OCR, ATP turnover and respiratory capacity of mitochondria (Fig. 5H). All these findings suggest the AMPK-dependent action of metformin to reverse the cytosolic and mitochondrial ROS changes and cell death under MGO stress.

Because metformin has been suggested to inhibit mitochondrial complex I of the mitochondrial respiratory chain, we investigated the role of complex I inhibition in the action of metformin. To achieve this, we used rotenone (an inhibitor of complex I) at concentration of 10 μM that was used to inhibit OCR in Figs. 3D, 4G and 5H. We found that rotenone did not affect MGO-induced cell death at 6 h (Fig. 6A) nor cytosolic ROS reduction at 2 and 4 h (Fig. 6B). Likewise, MGO-induced mitochondrial O_2^- and H_2O_2 production were not changed by rotenone (Fig. 6C and D). Next, we examined the effects of rotenone on AMPK activity. Of note, we found that 10 μM rotenone did not induce AMPK phosphorylation within 6 h (data not shown), and only a weak and delayed AMPK phosphorylation was detected under 25 μM rotenone treatment for 6 h (Fig. 6E). The quantification of Fig. 6E data was shown in the Supplementary Fig. 3. Because rotenone (10 μM) exerts effects different from metformin on AMPK activation, we exclude complex I inhibition as the mechanism by which metformin induces AMPK

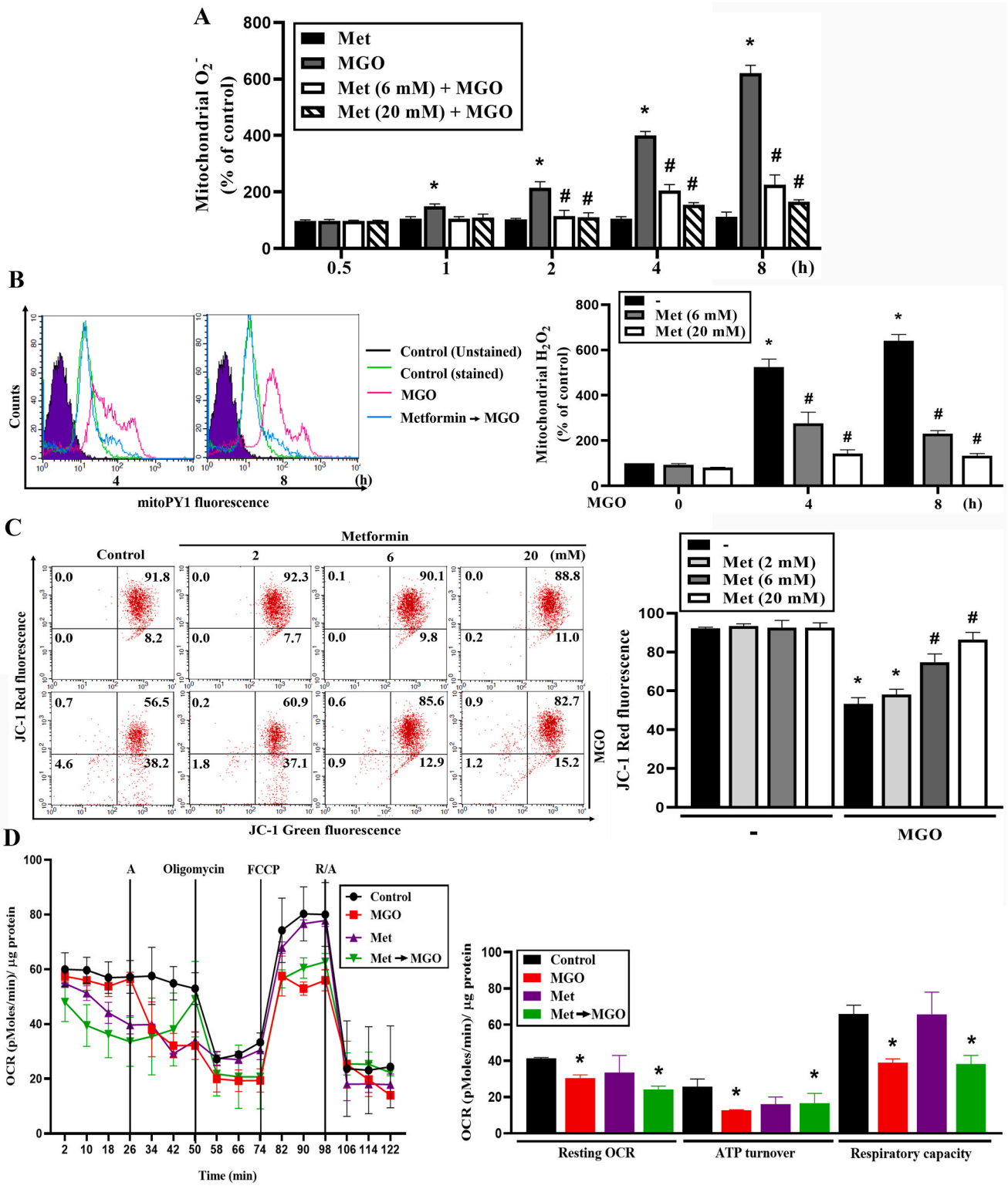

Fig. 3. Metformin attenuates MGO-induced mitochondrial ROS production and mitochondrial membrane potential loss.
(A, B) Cells were 30 min pretreated with metformin (6 mM or 20 mM) followed by MGO (300 µg/ml) stimulation for indicated time points. Mitochondrial superoxide anion and mitochondrial H_2O_2 were measured using mitoSOX **(A)** and mitoPY1 **(B)** respectively. **(C)** Cells were pretreated with metformin (2, 6 or 20 mM) 30 min prior to MGO (300 µg/ml) treatment. Four hours later JC-1 was used to measure the mitochondrial membrane potential by FACScalibur. **(D)** Cells were treated with metformin (6 mM) and immediately subjected into Seahorse XFe24 analyzer. After 26 min MGO was injected through port A. Cells were subsequently treated with oligomycin (2.5 µM), FCCP (1 µM) and antimycin A (2.5 µM)/rotenone (2.5 µM) through parts B, C and D at 50 min, 74 min and 98 min, respectively. Intracellular OCR was measured by seahorse XF24 analyzer. Data were the mean ± S.E.M. from at least 3 independent experiments. *$p < 0.05$, indicating the significant effect of MGO. #$p < 0.05$, indicating the reversal effects of metformin.

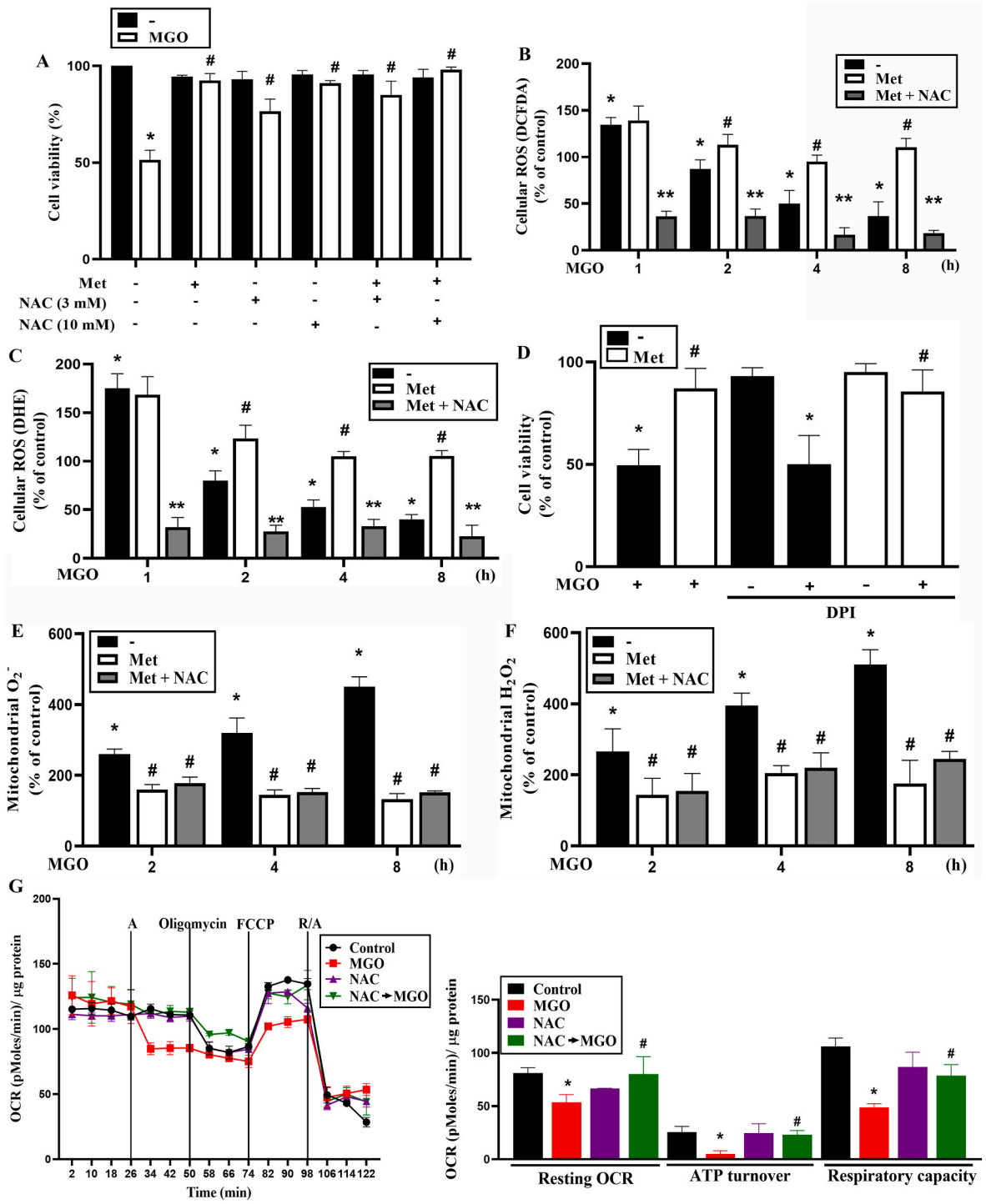

Fig. 4. Increase of mitoROS but not reduction of cytosolic ROS involves in MGO-induced cell death in ARPE-19 cells.
(A) Cells were 30 min pretreated with NAC (3 and 10 mM) prior to MGO (300 µg/ml) treatment for 6 h. Then Cell viability was determined. **(B, C, E, F)** Cells were 30 min pretreated with metformin (6 mM) and/or NAC (3 mM) followed by MGO (300 µg/ml) treatment for 4 h. DCFDA (B), DHE (C), mitoSOX (E), and mitoPY1 (F) were used to measure ROS. **(D)** Cells were 30 min pretreated with DPI (3 µM) and/or metformin (6 mM) prior to MGO (300 µg/ml) treatment for 6 h. Cell viability was measured. **(G)** Cells were treated with NAC (5 mM) and immediately subjected into Seahorse XFe24 analyzer for measurement of OCR as described in Fig. 3D. Data were the mean ± S.E.M. of at least 3 independent experiments. *$p < 0.05$, indicating the significant effect of MGO; #$p < 0.05$, indicating the reversal effects of metformin and NAC. **$p < 0.05$, indicating the significant reduction of ROS by NAC.

activation.

3.5. *Metformin and A769662 reverse MGO-induced mitochondrial fission, PGC-1α downregulation and autophagy inhibition*

Imbalances of mitochondrial dynamics (fission vs fusion) and mitochondrial mass (biogenesis vs mitophagy) contribute to cell death. We

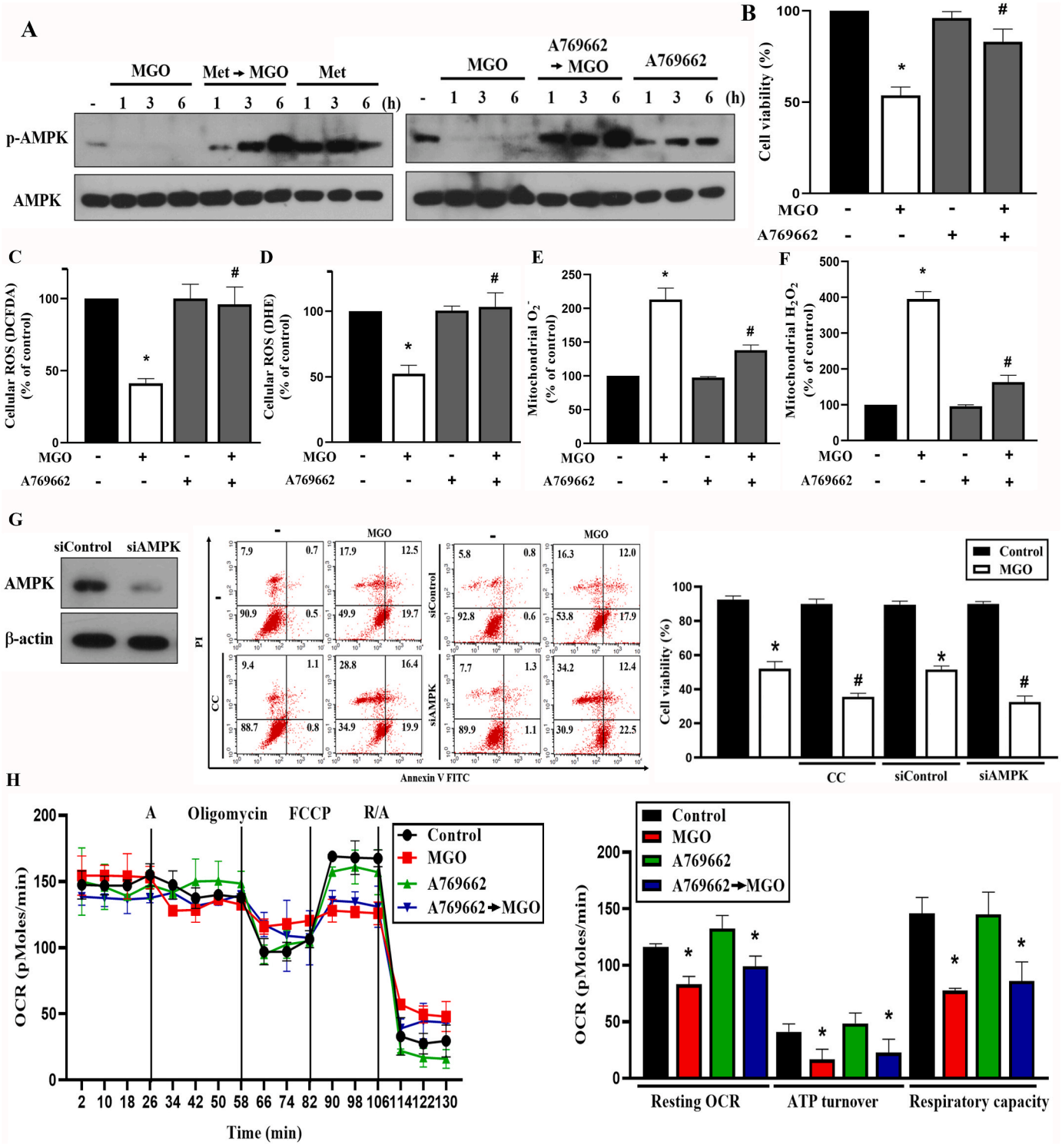

Fig. 5. AMPK activator A769662 mimics the effect of metformin in MGO-stimulated cells

(A) Cells were pretreated with metformin (6 mM) or A769662 (25 μM) 30 min prior to MGO (300 μg/ml) treatment for indicated time points. AMPK phosphorylation was measured by immunoblotting. **(B)** Cells were 30 min pretreated with A769662 (25 μM) prior to MGO (300 μg/ml) for 6 h. Cell viability was measured by Annexin V-FITC/PI using FACS. **(C, D, E, F)** Cells were pretreated with A769662 (25 μM) for 30 min followed by MGO (300 μg/ml) treatment for 4 h. DCFDA **(C)**, DHE **(D)**, mitoSOX **(E)**, and mitoPY1 **(F)** were used to measure cellular ROS. **(G)** Cells were 30 min pretreated with compound C (10 μM) followed by MGO (300 μg/ml) stimulation for 6 h. In some experiments, ARPE-19 cells were treated with siRNA followed by stimulation with MGO (300 μg/ml) for 6 h. Cell viability was measured by Annexin V-FITC/PI using FACS. AMPK expression after siRNA treatment was determined by immunoblotting. **(H)** Immediately after treatment with A769662 (25 μM), cells were subjected into SFe24 analyzer for OCR measurement, as described in Fig. 3D. Data were the mean ± S.E.M. from at least 3 independent experiments. *$p < 0.05$, indicating the significant effect of MGO; #$p < 0.05$, indicating the significant effects of A769662, compound C and AMPK silencing on MGO-induced responses.

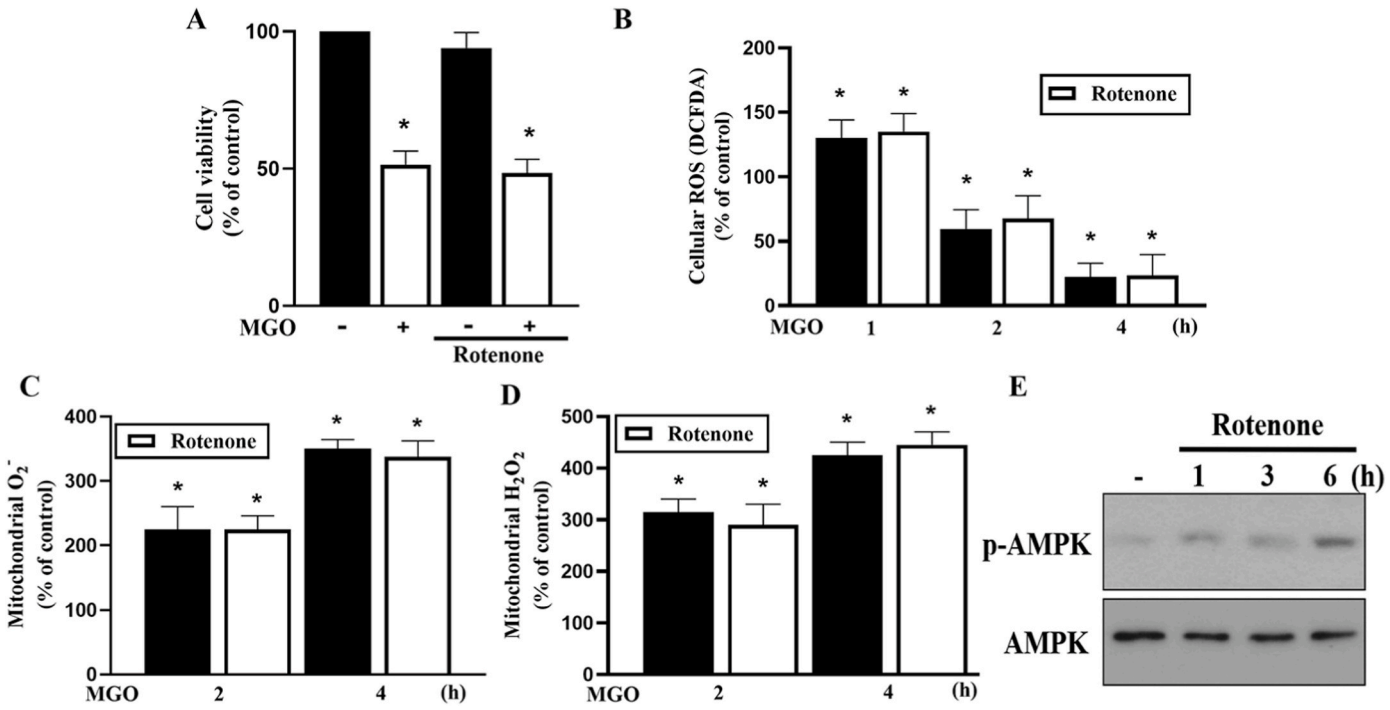

Fig. 6. Rotenone fails to affect the MGO-induced cellular responses.
(A) Cells were pretreated with rotenone (10 μM) 30 min prior to MGO (300 μg/ml) stimulation for 6 h. Cell viability was measured by Annexin V-FITC/PI using FACS. **(B–D)** Cells were pretreated with rotenone (10 μM) 30 min prior to MGO (300 μg/ml) stimulation for indicated times. DCFDA **(B)** mitoSOX **(C)** mitoPY1 **(D)** were used to measure cellular ROS. **(E)** Cells were treated with 25 μM rotenone for 1, 3 or 6 h. AMPK phosphorylation was determined by immunoblotting. Data were the mean ± S.E.M. from at least 3 independent experiments. *$p < 0.05$, indicating the significant effect of MGO.

first used Tom 20 staining in confocal microscopy and found that MGO treatment for 1 h increased mitochondrial fission, which is a process to undergo division or fragmentation into smaller mitochondria, and this process was prevented by metformin and A769662 (Fig. 7A). Biochemical immunoblotting of key proteins responsible for mitochondrial biogenesis and dynamics was determined. PGC-1α has merged as a master regulator of mitochondrial biogenesis, and has been shown to be activated by AMPK with phosphorylation at T172 and S538. PGC-1α mediates AMPK-dependent expression of mitochondrial genes including PGC-1α itself [39]. Our data revealed that PGC-1α protein was time-dependently downregulated by MGO and this change was prevented by metformin and A769662 (Fig. 7B). Moreover, we found MGO decreased MFN1 protein expression without affecting the protein levels of MFN2, OPA1 or Drp-1. We also did not detect the signal of Drp-1-S616 phosphorylation before or after metformin (or A769662) + MGO treatment. Moreover, the effect on downregulation of MFN1 was reversed by metformin and A769662 (Fig. 7B). The quantification of Fig. 7B data was shown in the Supplementary Fig. 4A. Also, MGO decreased PGC-1α and MFN1 mRNA levels and both effects were reversed by metformin and A769662 (Fig. 7C). In addition, MGO decreased TFAM gene expression (Fig. 7C), which is the major mitochondrial transcription factor to aid transcription of the mitochondrial genome. On the other hands, MFN2, OPA1 and Drp-1 mRNA levels were not altered by MGO, regardless of whether the cells were in the presence or not of either metformin or A769662 (Fig. 7C). To confirm these actions of metformin resulting from AMPK, we silenced AMPK and treated cells with compound C, an AMPK inhibitor. We found that AMPK silencing and compound C treatment significantly reduced PGC-1α protein expression (Fig. 7D), confirming PGC-1α is the downstream target of AMPK. Of note, the inhibitory effect of MGO on PGC-1α expression was still observed in compound C treatment condition, but not in cells where AMPK was silenced. (Fig. 7D). The quantification of Fig. 7D data was shown in the Supplementary Fig. 4B. These data suggest that MGO-induced AMPK inhibition leads to decrease mitochondrial biogenesis and induce mitochondrial fission.

Because AMPK-dependent autophagy/mitophagy confers a cell protective mechanism against $NaIO_3$ in ARPE cells [33], we tested the role of autophagy in the cell survival under MGO stress. We found that MGO time-dependently decreased LC3II protein expression and this effect was still observed by the co-treatment with bafilomycin A1 (Fig. 7E). The quantification of Fig. 7E data was shown in the Supplementary Fig. 4C. In addition, MGO itself did not inhibit the LC3 mRNA level regardless the presence of metformin and A769662 or not (Fig. 7C). These data suggest that MGO-induced AMPK inhibition also contributes to the reduction of autophagic flux, leading to mitochondrial dysfunction and cell death. Likewise, AMPK-dependent promotion of mitochondrial biogenesis and attenuation of mitochondrial fission underlie the protective actions of metformin and A769662.

3.6. *GLO1 downregulation by MGO is reversed by metformin and A769662*

The enzyme glyoxalase 1 (GLO1) is the main opponent in the degradation of the reactive MGO. To understand if GLO1 contributes to the effects of MGO and metformin, we treated cells with GLO1 inhibitor *S-p*-bromobenzylglutathione cyclopentyl diester (BBGC) or with GLO1 siRNA. We found that both treatments can sensitize cells to MGO-induced cell death (Fig. 8A and B). Moreover, the cell protective effects of metformin and A769662 were still observed upon BBGC treatment (Fig. 8A). Along with MGO treatment, GLO1 mRNA and protein expression were decreased, and metformin and A769662 can reverse this effect of MGO (Fig. 8C and D). The quantification of Fig. 8C data was shown in the Supplementary Fig. 5. In addition, GLO1 activity, but not GLO2 activity, was concomitantly reduced by MGO, and both metformin and A769662 can reverse this effect on GLO1 (Fig. 8E).

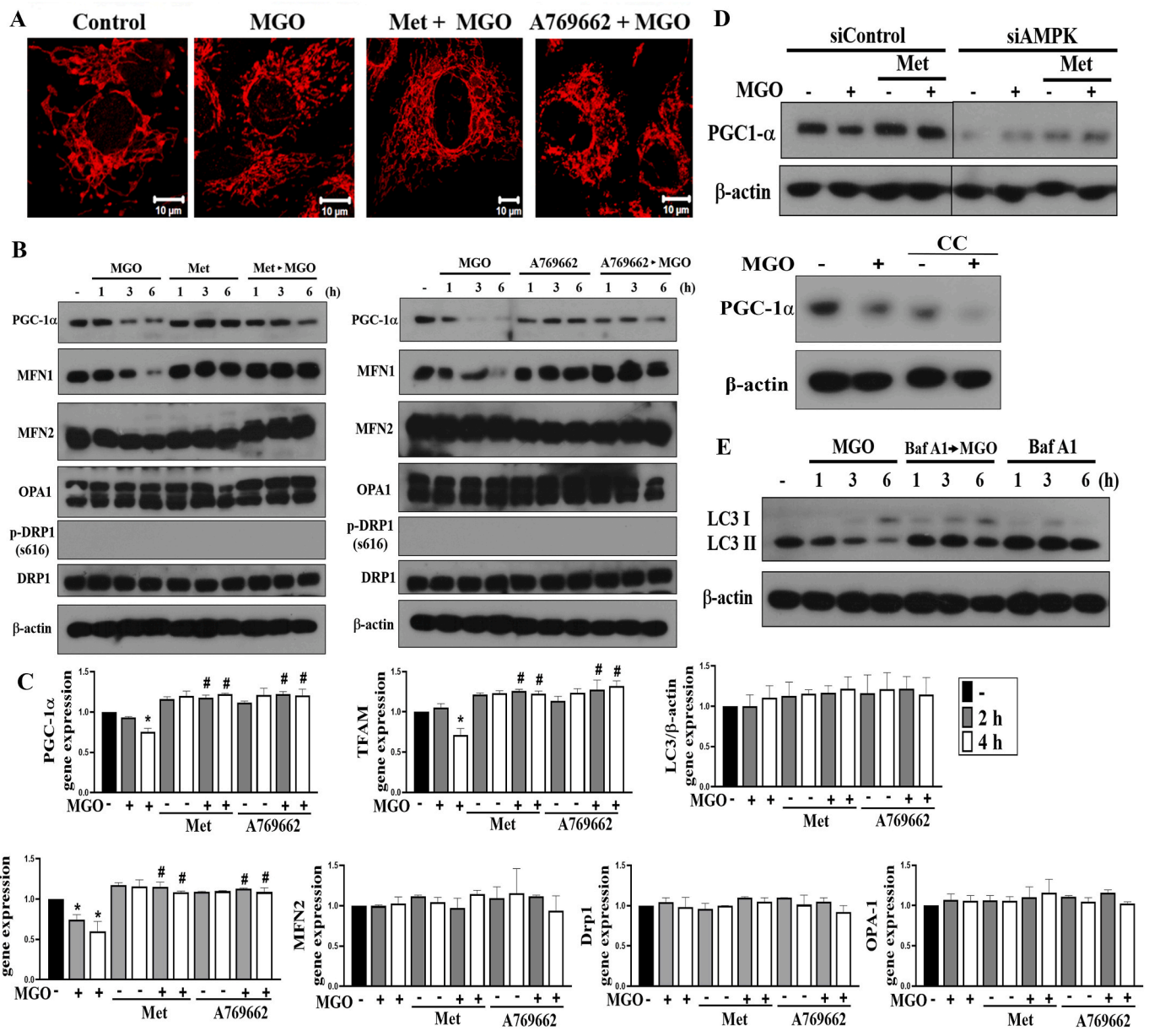

Fig. 7. Metformin and A769662 reverse MGO-induced mitochondrial fission and downregulation of mitochondrial biogenesis genes expression.
(A, B, C) Cells were pretreated with metformin (6 mM) and/or A769662 (25 μM) 30 min prior to MGO (300 μg/ml) stimulation. After 2 h, Tom20 staining was conducted and imaged (A). Scale bars indicated 10 μm. After 1, 3, or 6 h, cell lysates were prepared for immunoblotting (B). After 2 or 4 h, PGC-1α, TFAM, MFN1, MFN2, OPA1, Drp-1 and LC3 gene expressions were measured (C). **(D)** In some experiments, AMPK was silenced or was 30 min pretreated with compound C (10 μM) before MGO (300 μg/ml). After 3 h, PGC-1α protein expression was determined. **(E)** Cells were co-treated with bafilomycin A1 (100 nM) and/or MGO (300 μg/ml) for 1, 3, or 6 h, and then LC3 protein level was determined. *$p < 0.05$, indicating the significant effect of MGO. #$p < 0.05$, indicating the blockade effects of metformin and A769662.

3.7. Metformin and A769662 protect mice from MGO-induced retinopathy

To fully verify the cell protective action of metformin and A769662, we used intravitreal injection of each agent together with MGO in mice. After MGO treatment at 1.5 nmol for 24 h we did not observe significant changes in ERG, while we observed the ocular opaqueness and vision loss in mice at day 5. Therefore, we determined 3 days after the administration of MGO as the appropriate time in mice model. After injection for 3 days, we conducted ERG, fundus and OCT examinations. In ERG study, we found that MGO significantly diminished the a and b wave responses and increased the implicit time to b wave. These changes caused by MGO were reversed by the addition of either metformin or A769662 (Fig. 9A), confirming the effectiveness of intravitreal delivery of metformin and A769662 to maintain photoreceptor (a wave), bipolar and Müller cells (b-wave) functions in MGO-treated mice.

Moreover, the fundus examinations at day 3 post intravitreal injection revealed no abnormalities in PBS-treated mice. However, intravitreal injection of MGO induced multiple whitish patches of various sizes that were randomly scattered over the entire posterior pole (Fig. 9B). These whitish lesions were comparable with the cotton wool spots commonly observed in DR patients. Interestingly metformin and A769662 treatment with MGO ameliorated the induction of cotton wool spots-like whitish patches (Fig. 9B). Furthermore, cleaved caspase 3 detected by immunoblotting in MGO group was significantly reduced in metformin + MGO and A769662 + MGO treated mice (Fig. 9C). The

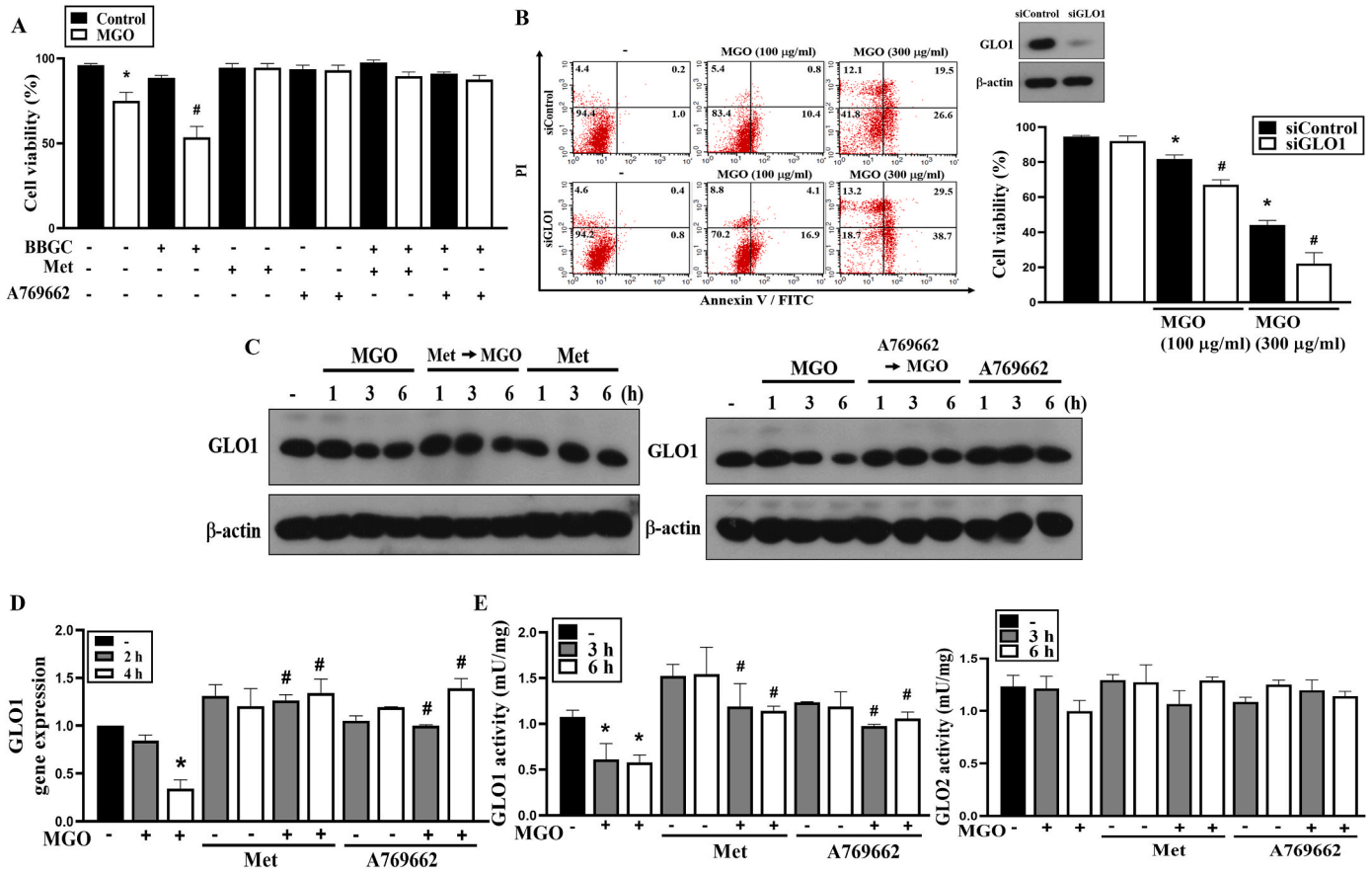

Fig. 8. Metformin and A769662 reverse MGO-induced GLO1 downregulation.
(A) Cells were pretreated with BBGC (10 μM), metformin (6 mM) and/or A769662 (25 μM) 30 min before MGO (100 μg/ml) stimulation. After 4 h, cell viability was determined by Annexin V-FITC/PI staining using FACS. **(B)** Cells were treated with siRNA to silence GLO1, then treated with MGO (100 or 300 μg/ml) for 6 h. Cell viability was determined by Annexin V-FITC/PI staining using FACS. **(C–E)** Cells were pretreated with metformin (6 mM) and/or A769662 (25 μM) 30 min prior to MGO (300 μg/ml) stimulation. **(C)** After incubation for 1, 3, or 6 h, cell lysates were prepared for immunoblotting. **(D)** After incubation for 2 or 4 h, GLO1 gene expression was measured using PCR analysis. **(E)** After incubation for 3 or 6 h, GLO1 and GLO2 activities were determined by commercial kits according to the manufacturer's instructions. Data were the mean ± S.E.M. from at least 3 independent experiments. *$p < 0.05$, indicating the significant effect of MGO. #$p < 0.05$, indicating the blockade effects of metformin and A769662.

quantification of Fig. 9C data was shown in the Supplementary Fig. 6.

To further elucidate the anatomical changes in MGO group, we conducted SD-OCT examinations at day 3 post intravitreal injections. All layers of the retina were clearly visible and no abnormalities were detected in the PBS group. As expected, in MGO group, subretinal deposits and disruption of IO/OS layers were seen (Fig. 10A). We could not find any unusual pathological conditions in metformin + MGO and A769662 + MGO group mice. In H&E staining, the mouse eyes at day 3 showed no abnormalities in PBS, metformin alone and A769662 alone groups. In MGO injected retina groups, obvious damage in RPE and ganglion cell layers, and decreased thickness in IPL and ONL were shown clearly. However, these features were not observed in metformin + MGO and A769662 + MGO group mice (Fig. 10B). These findings indicate that AMPK activation can protect the retina from MGO-induced functional impairments in photoreceptors, bipolar cells and Müller cells, as well as anatomical damage in the RPE and ganglion cell layers.

4. Discussion

Structural injury and dysfunction of the RPE are underlying factors in many inherited and acquired retinal diseases. Recently, the beneficial effects of metformin beyond insulin blood glucose lowering effect has been shown in anti-cancers [40], cardio-protection [41], hepatoprotection [42], and anti-ageing [43,44]. Moreover, use of metformin is effective in reducing oxidative stress [45]. Clinical data indicate that metformin may be a new therapeutic strategy for retinal diseases, including age-related macular degeneration (AMD) [17–21]. Although some studies have shown the beneficial effects of AMPK activation against MGO-induced oxidative stress and cell death in PC12 cells [46,47], pancreatic β-cells [48], endothelial cells [49], neuroblastoma cells [50–52] and cardiomyocytes [53], the detailed molecular mechanisms remain incomplete. Recently, metformin has been shown to protect ARPE-19 cells from glyoxal-induced oxidative stress and maintain the integrity of tight junctions of RPE cells in $NaIO_3$-treated rats [28]. The authors used a CCK-8 assay and demonstrated that 0.5 mM glyoxal induces about 25% ARPE-19 cell death, and metformin at concentrations up to 5 mM only reduces cytotoxicity by 10%. In addition, they found the TUNEL-positive cells are 2.2% in glyoxal group and are 0.5% in glyoxal + metformin group. In our study, we found that under significant cell death condition of MGO, i.e. around 50–60% cell death caused by 300 μg/ml MGO, metformin can concentration-dependently prevent this event with a total protection at 6 mM co-treatment with MGO. Moreover, we demonstrated several AMPK-dependent cellular events contributing to this protective effect of metformin. These include reductions of MGO-induced mitochondrial ROS production, mitochondrial membrane potential loss, mitochondrial fission, autophagy inhibition, mitochondrial biogenesis inhibition, and GLO1 downregulation. We also exclude the involvement of reduced cytosolic ROS levels in the death pathways of MGO. In addition, the AMPK activation by metformin is not associated with the inhibition of respiratory complex I in mitochondria.

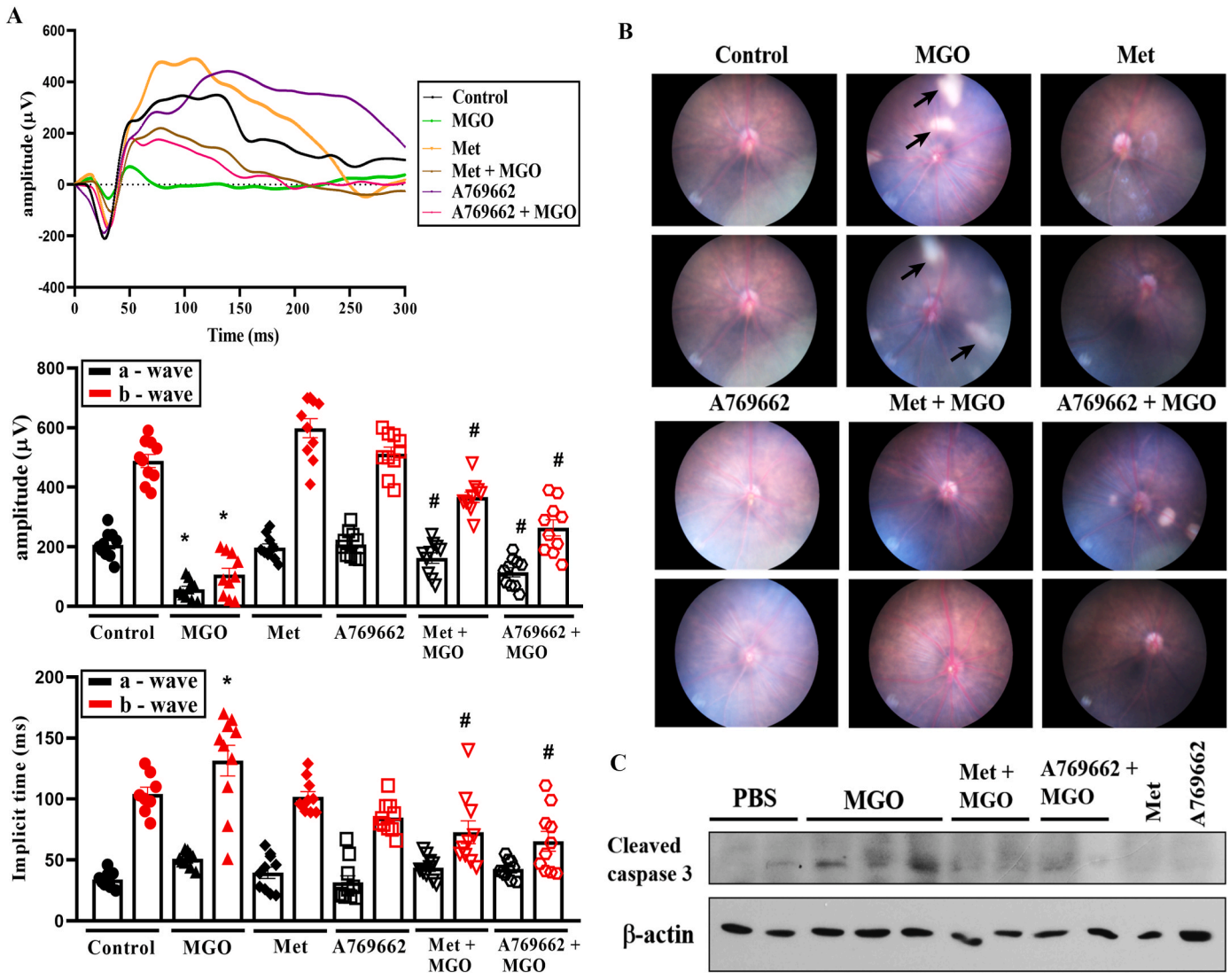

Fig. 9. Metformin and A769662 protect mice from MGO-induced retinopathy.
Aestheticized mice were intravitreally injected with PBS (n = 10), MGO (1.5 nmol) (n = 10), metformin (5 μg) (n = 10), metformin (5 μg) + MGO (1.5 nmol) (n = 10), A769662 (20 pmol) (n = 10), or A769662 (20 pmol) + MGO (1.5 nmol) (n = 10). At day 3 post injection, ERG waves **(A)** and fundus images **(B)** were recorded. The arrows indicate the cotton wool spots. Retina were euthanized from indicated mice groups and immunoblotting of lysates was conducted **(C)**. Data were the mean ± S.E.M. from 10 mice. *p < 0.05, indicating the significant effect of MGO; #p < 0.05, indicating the reversal effects of metformin and A769662.

Previous studies indicate metformin is a MGO scavenger [54,55], while beneficial action of metformin against MGO toxicity beyond scavenging property has also been proposed [56]. The supporting reason against physiologically scavenger action of metformin is the chemical reaction that MGO and metformin form imidazolinone requires an alkaline environment and a temperature of 4 °C [54]. Therefore, we examined the role of AMPK activation in the cell protective effect of metformin. Since AMPK specific activator A769662 showed similar findings of metformin, AMPK signal activation is suggested to be responsible for the action of metformin. Moreover, given that metformin (10 mM) post-treatment for up to 4 h still can exert similar protection efficacy as co-treatment for cell protection, we exclude the scavenger action of metformin as previously proposed. Therefore, we suggest AMPK activation is the major mechanism of metformin for the cell protection.

ROS are crucial signal messengers in cellular function. Although ROS are toxic agents, particularly in chronic conditions, they also play a beneficious role when present at low levels. These molecules are signal mediators of physiological responses and activate cell protective mechanisms upon injury. Therefore, the balance between oxidants and antioxidants should be finely regulated to avoid ROS reaching a damaging threshold [57]. It is well known that the most important risk factor associated with RPE injury is the oxidative stress. However, recently we confirmed the double-edged sword action of cytosolic ROS in RPE cells. We found that cytosolic ROS actually are required for autophagy formation in response to oxidative toxic agent $NaIO_3$. Dramatic attenuation of cytosolic ROS level in $NaIO_3$-treated RPE cells can enhance cell death via elimination of protective autophagy [33]. In MGO-treated RPE cells, even cytosolic ROS level is concomitantly decreased along with the increased mitochondrial ROS production, both events are in parallel reversed by metformin and A769662. Moreover, our findings with NAC and DPI exclude the assumed protective role of cytosolic ROS against MGO stress. In the studies with NAC, we found the metformin-induced cell viability can be maintained under the NAC + metformin condition with decreased cytosolic ROS. On the other hand, the NADPH oxidase inhibitor DPI which decreases cytosolic ROS still cannot affect the cell protective effect of metformin. Despite our data suggest attenuation of mitochondrial ROS production is the common and key protective mechanism for metformin, A769662 and NAC, it might exist different action mechanisms among AMPK activators and

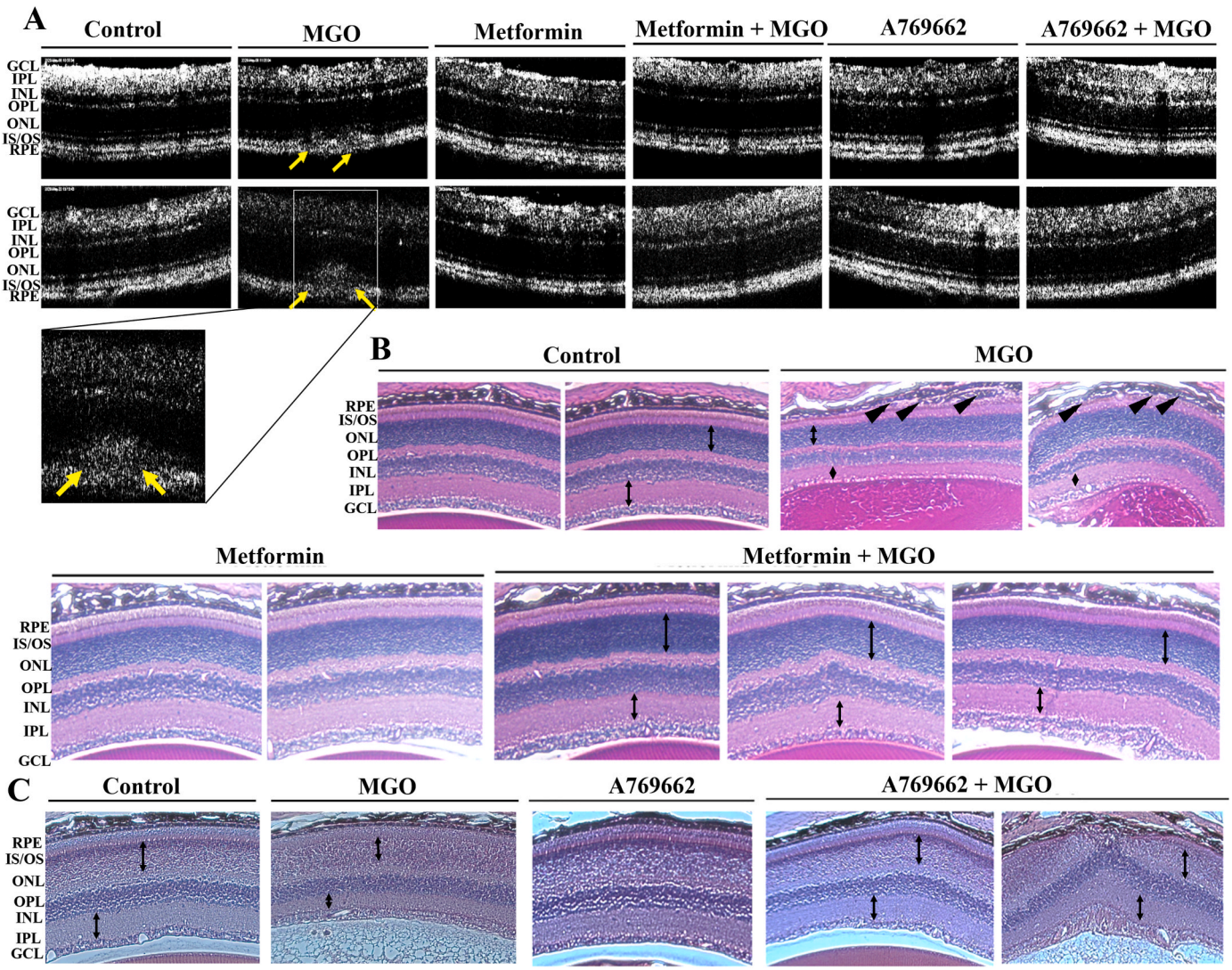

Fig. 10. Metformin and A769662 reverse MGO-induced changes of retinal morphology.
Aestheticized mice were intravitreally injected with PBS (n = 10), MGO (1.5 nmol) (n = 10), metformin (5 μg) (n = 10), metformin (5 μg) + MGO (1.5 nmol) (n = 10), A769662 (20 pmol) (n = 10), or A769662 (20 pmol) + MGO (1.5 nmol) (n = 10). At day 3 post injection, optical coherence tomographical images **(A)** and H&E staining images **(B)** were determined. The yellow arrows in (A) indicate subretinal deposits. The black bidirectional arrows in (B) indicate the thickness of IPL and ONL. The black arrowheads in (B) indicate the broken of RPE lining. (For interpretation of the references to color in this figure legend, the reader is referred to the Web version of this article.)

NAC. NAC can restore the inhibitory effect of MGO on oxidative phosphorylation, while metformin and A769662 cannot. More detailed cellular context-dependent molecular mechanisms that integrate the complicated cellular events caused by MGO, AMPK activators and NAC need more investigation in the future. Regarding to the effect of MGO to decrease cytosolic ROS, we speculate it might result from the regulation of cellular GSH level as previously reported [58–60]. In this aspect, we detected higher intracellular GSH level after MGO treatment within 4 h (data not shown). Taken together, currently we do not have sufficient evidence to understand the role of cytosolic ROS in the cellular responses under different oxidative stress conditions.

Mitochondria are essential organelles that supply energy to the cells through oxidative phosphorylation (OXPHOS) and are also essential in calcium buffering, cell cycle control and regulation of apoptosis. Under stress, a delicate balance between both mitochondrial fission and fusion is required to maintain functional mitochondria. An excess of mitochondrial fission leads to mitochondrial fragmentation, and failure in any of the components of the machinery in controlling mitochondrial dynamics may lead to RPE degeneration [61]. Previously MGO has been shown to induce mitochondrial fission in retinal endothelial cells [62], but the underlying mechanisms remain unknown. In agreement with this study in endothelial cells, MGO can trigger mitochondrial fission in ARPE-19 cells. We further showed MGO can specifically affect molecules involving to regulate mitochondrial dynamics. MGO can downregulate MFN1 gene and protein expression, without affecting MFN2, OPA1 or Drp1 in ARPE-19 cells. Although currently we cannot provide sufficient answers for the specific action of MGO in these mitochondrial dynamic regulators, our findings indicate an AMPK-dependent mechanism in regulating MFN1 gene expression. One study has demonstrated the role of AMPK in upregulation of MFN1 [63]. In addition, distinct functions between MFN1 and MFN2 might exist, which is also worthy for further investigation. Previously it was shown that OPA1 requires MFN1, but not MFN2, to regulate the fusion process [64]. Altogether, MGO-induced downregulation of MFN1 via inhibition of AMPK might lead to the unbalance of mitochondrial dynamics and induce mitochondrial stress for cell apoptosis.

To maintain intact mitochondrial morphology, both mitochondrial biogenesis and mitophagy are as crucial as mitochondrial dynamics in

RPE cells. In this study, we found that the major mitochondrial biogenesis factors PGC-1α and TFAM are downregulated by MGO and both inhibitions can be reversed by AMPK activator. We suggest MGO can induce the insufficient supply of newly synthesis of young mitochondria to support cellular stress. Moreover, autophagy is a conserved cell survival pathway that catabolizes damaged proteins and organelles to maintain homeostasis. Mitophagy is a mitochondria-specific type of autophagy and is essential for mitochondrial quality control and homeostasis. Numerous studies have demonstrated that autophagy is highly active in the RPE, and sustained autophagy dysfunction, particularly in mitophagy and lysosomal rupture, is associated to DR, RPE degeneration and irreversible blinding diseases [21,61,65–67]. In this study, we found the effect of MGO to suppress the autophagic flux key player LC3II without affecting LC3 gene transcription. Taken together, we suggest the imbalance of mitochondrial morphology resulting from inhibition of mitochondrial biogenesis and mitophagy, but excess mitochondrial fission, contributes to MGO-induced cell death in RPE cells. Even though mitochondrial respiration is suppressed by MGO, this event is not rescued by the AMPK-dependent actions of metformin and A769662. In this context, previous studies have also demonstrated the dissociation between mitochondrial oxidative phosphorylation and mitochondrial ROS-dependent cell death [68]. We assume the suppression of mitochondrial phosphorylation may be an adaptive pathway to maintain cellular viability in response to oxidative stress.

AMPK is an evolutionarily conserved master kinase that plays a crucial role in multiple cell functions, including cell metabolism, energy homeostasis, cell growth, inflammation, infection, redox regulation, tissue repair, and regeneration [69–71]. Recently, AMPK activity has been demonstrated to protect RPE cells from various insults, such as UV radiation [72], hydrogen peroxide [73], photoreceptor outer segment [74], $NaIO_3$ [32], and hypoxia [75], and delay inherited retinal degeneration [30]. Although MGO has been shown to activate AMPK-autophagy axis in PC12 cells [76], we observe the inhibitory effect of MGO on AMPK in RPE cells. In addition, we confirmed the general protective role of AMPK in stressed RPE cells. In this study, the AMPK-associated protective mechanisms to reduce MGO stress and maintain mitochondrial dynamic homeostasis, including suppression of mitochondrial fission, as well as enhancement of mitochondrial biogenesis and autophagy, result from its positive effects on upregulation of PGC-1α, MFN1 and TFAM gene expression [39,63,77–79]. Besides protection of RPE cells against oxidative stress, it is an interesting issue to elucidate the role of AMPK in RPE cell migration in the future. This is because both disruption of RPE barrier integrity and RPE migration are hallmark features in numerous retinal diseases [80,81].

GLO1 acts as an *anti*-glycation defense system by detoxifying MGO, thus drawing recent attention to its pathological role. Modulation of GLO1 pathway provides a new treatment strategy against AGE-associated complications [82], including DR [83,84]. Moreover, glycation of GLO1 is involved in several diseases such as diabetes, obesity, atherosclerosis, cancers and age-related diseases [82,85–87]. Reduced GLO1 in human atherosclerotic plaques is highly linked to MGO and AGE accumulation, inflammation, and subsequent apoptosis and rupture of plaques in diabetes [88,89]. In contrast, higher GLO1 expression and activity alleviate dicarbonyl stress, leading to slow the development of obesity, insulin resistance, DR and other microvascular complications of diabetes. It has been shown that treatment of patients with type 2 diabetes by metformin leads to decrease plasma MGO level, increase GLO1 activity in peripheral mononuclear cells, red blood cells [55] and atherosclerotic lesions [89]. In this study, our data reveal metformin can directly upregulate GLO1 expression via AMPK-dependent pathway. This finding is consistent to previous notion of AMPK-dependent GLO1 expression via AMPK-Nrf2-ARE axis [90,91]. To date developing small-molecule inducers of GLO1 expression and activation such as *trans*-resveratrol-hesperetin combination [92], dihydromyricetin [46], marein [47], and L-cysteine [93] becomes a promising strategy to prevent diabetes associated complications. Our data also strengthen the potential therapeutic target of GLO1 in the prevention of diabetic complications.

5. Conclusion

In summary, we demonstrate that MGO not only induces mitochondrial fission, mitochondrial ROS production, and mitochondrial membrane potential loss, but also inhibits autophagy, mitochondrial biogenesis and GLO1 expression in RPE cells. Metformin and AMPK activators can protect RPE cells from MGO-induced cell death by reversing above cellular stress events (Fig. 11). Moreover, the protective effect of metformin on retinopathy is evidenced in mice. Therefore, our findings suggest AMPK as a therapeutic target to directly ameliorate oxidative stress-induced retinal pigment epithelial injury and diabetic retinopathy.

Author contributions

W.W.L., P.S., and C.M.C., conceptualized, designed the study and wrote the manuscript. P.S., S.H.H. and D.Y.H. performed the experiments and analyzed the data. G.H. provided the technical support.

Funding

We like to thank the research funding from the Ministry of Science and Technology (MOST 110-2314-B-567-003-MY3), Cardinal Tien Hospital (CTH110A-2217), and National Taiwan University College of Medicine (NSCCMOH-145-61). We would like to acknowledge the service provided by the Immune Research Core of Department of Medical Research at National Taiwan University Hospital and the imaging core in the First Core Labs at the National Taiwan University, College of Medicine.

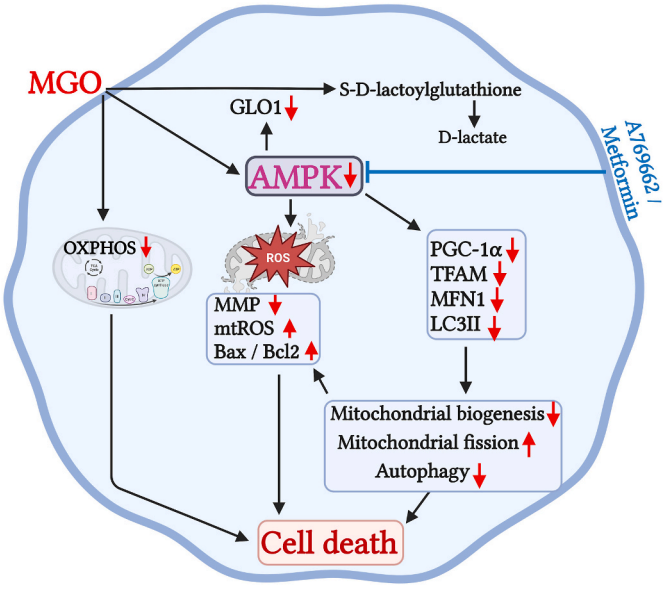

Fig. 11. Schematic summary of the cell protective actions of metformin and A769662 in MGO-treated ARPE-19 cells via AMPK activation. MGO can inhibit AMPK, leading to downregulation of MFN1, PGC-1α and TFAM gene expression and inhibition of LC3II/I ratio. These events cause mitochondrial fission, inhibit mitochondrial biogenesis and autophagy, which are accompanied by the mitochondrial dysfunction, ROS production, mitochondrial membrane potential loss, and caspase 3 activation. MGO can also downregulate GLO1 gene expression and inhibition of GLO1 activity leads to delay intracellular MGO metabolism and prolong its cytotoxicity. Metformin and A769662 can reverse above death pathway events of MGO through AMPK activation and protect RPE cells against MGO insult.

Declaration of competing interest

The authors declare that they have no known competing financial interests or personal relationships that could have appeared to influence the work reported in this paper.

Data availability

Data will be made available on request.

Abbreviations:

AGEs	advanced glycation end products
AMD	age-related macular degeneration
AMPK	adenosine monophosphate-activated protein kinase
ATP	adenosine triphosphate
BBGC	*S-p*-bromobenzylglutathione cyclopentyl diester
cDNA	complementary deoxyribonucleic acid
DCFDA	dichlorofluorescein diacetate
DHE	dihydroethidium
DMEM/F12	Dulbecco's Modified Eagle's Medium/Nutrient Mixture F-12
DM	diabetes mellitus
DPI	diphenyleneiodonium
DRP	dynamin-related protein
ERG	electroretinography
FCCP	carbonyl cyanide-*p*-trifluoromethoxyphenylhydrazone
FITC	fluorescein isothiocyanate
GLO	glyoxalase
H_2O_2	hydrogen peroxide
3-MA	3-methyladenine
MFN	mitofusin
MGO	methylglyoxal
MMP	mitochondrial membrane potential
mtROS	mitochondrial reactive oxygen species
NAC	N-acetylcysteine
NADPH	nicotinamide adenine dinucleotide phosphate
Nrf2	nuclear factor erythroid 2-related factor 2
O_2^-	superoxide anion
OCR	oxygen consumption rate
OPA1	optic atrophy-1
PBS	phosphate buffer saline
PCR	polymerase chain reaction
PGC-1α	peroxisome proliferator-activated receptor gamma coactivator *1-alpha*
PI	propidium iodide
ROS	reactive oxygen species
RPE	retinal pigment epithelium
SD-OCT	spectral domain optical coherence tomography
TBST	tris buffered saline
TFAM	Mitochondrial transcription factor A

Appendix A. Supplementary data

Supplementary data to this article can be found online at https://doi.org/10.1016/j.redox.2023.102786.

References

[1] J. Hanus, C. Anderson, S. Wang, RPE necroptosis in response to oxidative stress and in AMD, Ageing Res. Rev. 24 (Pt B) (2015) 286–298.
[2] A. Lakkaraju, A. Umapathy, L.X. Tan, et al., The cell biology of the retinal pigment epithelium, Prog. Retin. Eye Res. (2020), 100846.
[3] A.W. Stitt, AGEs and diabetic retinopathy, Invest. Ophthalmol. Vis. Sci. 51 (10) (2010) 4867–4874.
[4] H. Vlassara, J. Uribarri, Advanced glycation end products (AGE) and diabetes: cause, effect, or both? Curr. Diabetes Rep. 14 (1) (2014) 453.
[5] C.G. Schalkwijk, C.D.A. Stehouwer, Methylglyoxal, a highly reactive dicarbonyl compound, in diabetes, its vascular complications, and other age-related diseases, Physiol. Rev. 100 (1) (2020) 407–461.
[6] M.P. Kalapos, Where does plasma methylglyoxal originate from? Diabetes Res. Clin. Pract. 99 (3) (2013) 260–271.
[7] X. Kong, M.Z. Ma, K. Huang, et al., Increased plasma levels of the methylglyoxal in patients with newly diagnosed type 2 diabetes 2, J. Diabetes 6 (6) (2014) 535–540.
[8] M. Akagawa, A. Mori, K. Sakamoto, T. Nakahara, Methylglyoxal impairs beta2-adrenoceptor-mediated vasodilatory mechanisms in rat retinal arterioles, Biol. Pharm. Bull. 41 (2) (2018) 272–276.
[9] S. Di Loreto, V. Zimmitti, P. Sebastiani, et al., Methylglyoxal causes strong weakening of detoxifying capacity and apoptotic cell death in rat hippocampal neurons, Int. J. Biochem. Cell Biol. 40 (2) (2008) 245–257.
[10] K.D. Yoon, K. Yamamoto, K. Ueda, et al., A novel source of methylglyoxal and glyoxal in retina: implications for age-related macular degeneration, PLoS One 7 (7) (2012), e41309.
[11] Y. Sook Kim, I. Soo Lee, J. Sook Kim, Protective effects of puerariae radix extract and its single compounds on methylglyoxal-induced apoptosis in human retinal pigment epithelial cells, J. Ethnopharmacol. 152 (3) (2014) 594–598.
[12] M. Sousa Silva, R.A. Gomes, A.E. Ferreira, et al., The glyoxalase pathway: the first hundred years and beyond, Biochem. J. 453 (1) (2013) 1–15.
[13] Y.C. Chang, M.C. Hsieh, H.J. Wu, et al., Methylglyoxal, a reactive glucose metabolite, enhances autophagy flux and suppresses proliferation of human retinal pigment epithelial ARPE-19 cells, Toxicol. Vitro 29 (7) (2015) 1358–1368.
[14] J. Kim, C.S. Kim, Y.M. Lee, et al., Methylglyoxal induces hyperpermeability of the blood-retinal barrier via the loss of tight junction proteins and the activation of matrix metalloproteinases, Graefes Arch. Clin. Exp. Ophthalmol. 250 (5) (2012) 691–697.
[15] P. Zizkova, J. Viskupicova, V. Heger, et al., Dysfunction of SERCA pumps as novel mechanism of methylglyoxal cytotoxicity, Cell Calcium 74 (2018) 112–122.
[16] C.M. Chan, D.Y. Huang, Y.P. Huang, et al., Methylglyoxal induces cell death through endoplasmic reticulum stress-associated ROS production and mitochondrial dysfunction, J. Cell Mol. Med. 20 (9) (2016) 1749–1760.
[17] J.M. Stewart, R. Lamy, F. Wu, J.D. Keenan, Relationship between oral metformin use and age-related macular degeneration, Ophthalmol. Retina 4 (11) (2020) 1118–1119.
[18] A.L. Blitzer, S.A. Ham, K.A. Colby, D. Skondra, Association of metformin use with age-related macular degeneration: a case-control study, JAMA Ophthalmol 139 (3) (2021) 302–309.
[19] S.V. Amin, S. Khanna, S.P. Parvar, et al., Metformin and retinal diseases in preclinical and clinical studies: insights and review of literature, Exp. Biol. Med. (Maywood, NJ, U. S.) 247 (4) (2022) 317–329.
[20] J. Jiang, Y. Chen, H. Zhang, et al., Association between metformin use and the risk of age-related macular degeneration in patients with type 2 diabetes: a retrospective study, BMJ Open 12 (4) (2022), e054420.
[21] K.A. Vessey, A.I. Jobling, M.X. Tran, et al., Treatments targeting autophagy ameliorate the age-related macular degeneration phenotype in mice lacking APOE (apolipoprotein E), Autophagy 18 (10) (2022) 1–17.
[22] K.R. Dang, T. Wu, Y.N. Hui, H.J. Du, Newly-found functions of metformin for the prevention and treatment of age-related macular degeneration, Int. J. Ophthalmol. 14 (8) (2021) 1274–1280.
[23] C. Niu, Z. Chen, K.T. Kim, et al., Metformin alleviates hyperglycemia-induced endothelial impairment by downregulating autophagy via the Hedgehog pathway, Autophagy 15 (5) (2019) 843–870.
[24] Q.Y. Yi, G. Deng, N. Chen, et al., Metformin inhibits development of diabetic retinopathy through inducing alternative splicing of VEGF-A, Am. J. Transl. Res. 8 (9) (2016) 3947–3954.
[25] H. Zou, C. Shan, L. Ma, et al., Polarity and epithelial-mesenchymal transition of retinal pigment epithelial cells in proliferative vitreoretinopathy, PeerJ 8 (2020), e10136.
[26] C.W. Shu, C.L. Tsen, M.S. Li, et al., Metformin and rapamycin protect cells from vital dye-induced damage in retinal pigment epithelial cells and in vivo, Graefes Arch. Clin. Exp. Ophthalmol. 258 (3) (2020) 557–564.
[27] S.A. Eltony, H.S. Mohaseb, A.A. Ahmed, M.M. Sayed, Can metformin modulate the retinal degenerative changes in a rat model of retinitis pigmentosa? Tissue Cell 76 (2022), 101786.
[28] S. Qu, C. Zhang, D. Liu, et al., Metformin protects ARPE-19 cells from glyoxal-induced oxidative stress, Oxid. Med. Cell. Longev. 2020 (2020), 1740943.
[29] L. Xu, E.E. Brown, C.P. Santiago, et al., Retinal homeostasis and metformin-induced protection are not affected by retina-specific Ppardelta knockout, Redox Biol. 37 (2020), 101700.
[30] L. Xu, L. Kong, J. Wang, J.D. Ash, Stimulation of AMPK prevents degeneration of photoreceptors and the retinal pigment epithelium, Proc. Natl. Acad. Sci. U. S. A. 115 (41) (2018) 10475–10480.
[31] Y. Zhang, F. Chen, L. Wang, Metformin inhibits development of diabetic retinopathy through microRNA-497a-5p, Am. J. Transl. Res. 9 (12) (2017) 5558–5566.
[32] C.M. Chan, P. Sekar, D.Y. Huang, S.H. Hsu, W.W. Lin, Different effects of metformin and A769662 on sodium iodate-induced cytotoxicity in retinal pigment epithelial cells: distinct actions on mitochondrial fission and respiration, Antioxidants (Basel) 9 (11) (2020) 1057.
[33] C.M. Chan, D.Y. Huang, P. Sekar, S.H. Hsu, W.W. Lin, Reactive oxygen species-dependent mitochondrial dynamics and autophagy confer protective effects in retinal pigment epithelial cells against sodium iodate-induced cell death, J. Biomed. Sci. 26 (1) (2019) 40.

[34] F.L. Lin, C.H. Lin, J.D. Ho, et al., The natural retinoprotectant chrysophanol attenuated photoreceptor cell apoptosis in an N-methyl-N-nitrosourea-induced mouse model of retinal degenaration, Sci. Rep. 7 (2017), 41086.
[35] P. Sekar, G. Hsiao, Y.S. Chen, W.W. Lin, C.M. Chan, P2X7 is involved in the mouse retinal degeneration via the coordinated actions in different retinal cell types, Antioxidants (Basel) 12 (1) (2023) 141.
[36] P. Sekar, D.Y. Huang, S.L. Hsieh, S.F. Chang, W.W. Lin, AMPK-dependent and independent actions of P2X7 in regulation of mitochondrial and lysosomal functions in microglia, Cell Commun. Signal. 16 (1) (2018) 83.
[37] W.J. Jeong, J.H. Rho, Y.G. Yoon, et al., Cytoplasmic and nuclear anti-apoptotic roles of alphaB-crystallin in retinal pigment epithelial cells, PLoS One 7 (9) (2012), e45754.
[38] S.I. Dikalov, D.G. Harrison, Methods for detection of mitochondrial and cellular reactive oxygen species, Antioxidants Redox Signal. 20 (2) (2014) 372–382.
[39] S. Jager, C. Handschin, J. St-Pierre, B.M. Spiegelman, AMP-activated protein kinase (AMPK) action in skeletal muscle via direct phosphorylation of PGC-1alpha, Proc. Natl. Acad. Sci. U. S. A. 104 (29) (2007) 12017–12022.
[40] K. He, H. Hu, S. Ye, et al., The effect of metformin therapy on incidence and prognosis in prostate cancer: a systematic review and meta-analysis, Sci. Rep. 9 (1) (2019) 2218.
[41] X. Yu, D. Jiang, J. Wang, et al., Metformin prescription and aortic aneurysm: systematic review and meta-analysis, Heart 105 (17) (2019) 1351–1357.
[42] M. Iranshahy, R. Rezaee, G. Karimi, Hepatoprotective activity of metformin: a new mission for an old drug? Eur. J. Pharmacol. 850 (2019) 1–7.
[43] K. Mortezaee, D. Shabeeb, A.E. Musa, M. Najafi, B. Farhood, Metformin as a radiation modifier; implications to normal tissue protection and tumor sensitization, Curr. Clin. Pharmacol. 14 (1) (2019) 41–53.
[44] Z. Lv, Y. Guo, Metformin and its benefits for various diseases, Front. Endocrinol. (Lausanne) 11 (2020) 191.
[45] A. Esteghamati, D. Eskandari, H. Mirmiranpour, et al., Effects of metformin on markers of oxidative stress and antioxidant reserve in patients with newly diagnosed type 2 diabetes: a randomized clinical trial, Clin. Nutr. 32 (2) (2013) 179–185.
[46] B. Jiang, L. Le, H. Pan, et al., Dihydromyricetin ameliorates the oxidative stress response induced by methylglyoxal via the AMPK/GLUT4 signaling pathway in PC12 cells, Brain Res. Bull. 109 (2014) 117–126.
[47] B. Jiang, L. Le, H. Liu, et al., Marein protects against methylglyoxal-induced apoptosis by activating the AMPK pathway in PC12 cells, Free Radic. Res. 50 (11) (2016) 1173–1187.
[48] K.S. Suh, S. Chon, W.W. Jung, E.M. Choi, Magnolol protects pancreatic beta-cells against methylglyoxal-induced cellular dysfunction, Chem. Biol. Interact. 277 (2017) 101–109.
[49] S. Kim, S. Kim, A.R. Hwang, et al., Apelin-13 inhibits methylglyoxal-induced unfolded protein responses and endothelial dysfunction via regulating AMPK pathway, Int. J. Mol. Sci. 21 (11) (2020) 4069.
[50] M.C. Lai, W.Y. Liu, S.S. Liou, I.M. Liu, A bibenzyl component moscatilin mitigates glycation-mediated damages in an SH-SY5Y cell model of neurodegenerative diseases through AMPK activation and RAGE/NF-kappaB pathway suppression, Molecules 25 (19) (2020) 4574.
[51] M.R. de Oliveira, I.C.C. de Souza, F.B. Brasil, Promotion of mitochondrial protection by emodin in methylglyoxal-treated human neuroblastoma SH-SY5Y cells: involvement of the AMPK/Nrf2/HO-1 Axis, Neurotox. Res. 39 (2) (2021) 292–304.
[52] F.B. Brasil, F.J.S. de Almeida, M.D. Luckachaki, et al., The C-glucosyl flavone isoorientin pretreatment attenuates the methylglyoxal-induced mitochondrial dysfunction in the human neuroblastoma SH-SY5Y cells: role for the AMPK-PI3K/Akt/Nrf2/gamma-GCL/GSH axis, Metab. Brain Dis. 38 (2) (2022) 437–452.
[53] D.H. Nam, J.H. Han, S. Kim, et al., Activated protein C prevents methylglyoxal-induced endoplasmic reticulum stress and cardiomyocyte apoptosis via regulation of the AMP-activated protein kinase signaling pathway, Biochem. Biophys. Res. Commun. 480 (4) (2016) 622–628.
[54] O.R. Kinsky, T.L. Hargraves, T. Anumol, et al., Metformin scavenges methylglyoxal to form a novel imidazolinone metabolite in humans, Chem. Res. Toxicol. 29 (2) (2016) 227–234.
[55] C. Solis-Calero, J. Ortega-Castro, A. Hernandez-Laguna, J. Frau, F. Munoz, A DFT study of the carboxymethyl-phosphatidylethanolamine formation from glyoxal and phosphatidylethanolamine surface. Comparison with the formation of N(epsilon)-(carboxymethyl)lysine from glyoxal and L-lysine, Phys. Chem. Chem. Phys. 17 (12) (2015) 8210–8222.
[56] Z. Kender, T. Fleming, S. Kopf, et al., Effect of metformin on methylglyoxal metabolism in patients with type 2 diabetes, Exp. Clin. Endocrinol. Diabetes 122 (5) (2014) 316–319.
[57] B.D. E, G. Marfany, The relevance of oxidative stress in the pathogenesis and therapy of retinal dystrophies, Antioxidants (Basel) 9 (4) (2020) 347.
[58] L. de Bari, A. Scire, C. Minnelli, et al., Interplay among oxidative stress, methylglyoxal pathway and S-glutathionylation, Antioxidants (Basel) 10 (1) (2020) 19.
[59] M. Mari, E. de Gregorio, C. de Dios, et al., Mitochondrial glutathione: recent insights and role in disease, Antioxidants (Basel) 9 (10) (2020) 909.
[60] I. Allaman, M. Belanger, P.J. Magistretti, Methylglyoxal, the dark side of glycolysis, Front. Neurosci. 9 (2015) 23.
[61] K. Kaarniranta, H. Uusitalo, J. Blasiak, et al., Mechanisms of mitochondrial dysfunction and their impact on age-related macular degeneration, Prog. Retin. Eye Res. 79 (2020), 100858.
[62] S. Qian, Y. Qian, D. Huo, et al., Tanshinone IIa protects retinal endothelial cells against mitochondrial fission induced by methylglyoxal through glyoxalase 1, Eur. J. Pharmacol. 857 (2019), 172419.
[63] J. Gao, H. Wang, Y. Li, W. Li, Resveratrol attenuates cerebral ischaemia reperfusion injury via modulating mitochondrial dynamics homeostasis and activating AMPK-Mfn1 pathway, Int. J. Exp. Pathol. 100 (5–6) (2019) 337–349.
[64] S. Cipolat, O. Martins de Brito, B. Dal Zilio, L. Scorrano, OPA1 requires mitofusin 1 to promote mitochondrial fusion, Proc. Natl. Acad. Sci. U. S. A. 101 (45) (2004) 15927–15932.
[65] J.M.T. Hyttinen, J. Viiri, K. Kaarniranta, J. Blasiak, Mitochondrial quality control in AMD: does mitophagy play a pivotal role? Cell. Mol. Life Sci. 75 (16) (2018) 2991–3008.
[66] E. Keeling, A.J. Lotery, D.A. Tumbarello, J.A. Ratnayaka, Impaired cargo clearance in the retinal pigment epithelium (RPE) underlies irreversible blinding diseases, Cells 7 (2) (2018) 16.
[67] L.M. Lewis Lujan, M.F. McCarty, J.J. Di Nicolantonio, et al., Nutraceuticals/drugs promoting mitophagy and mitochondrial biogenesis may combat the mitochondrial dysfunction driving progression of dry age-related macular degeneration, Nutrients 14 (9) (2022) 1985.
[68] L.T. Chen, C.T. Lin, L.Y. Lin, et al., Neuronal mitochondrial dynamics coordinate systemic mitochondrial morphology and stress response to confer pathogen resistance in C. elegans, Dev. Cell 56 (12) (2021) 1770–1785.
[69] P. Silwal, J.K. Kim, J.M. Yuk, E.K. Jo, AMP-activated protein kinase and host defense against infection, Int. J. Mol. Sci. 19 (11) (2018) 3495.
[70] D.M. Thomson, The role of AMPK in the regulation of skeletal muscle size, hypertrophy, and regeneration, Int. J. Mol. Sci. 19 (10) (2018) 3125.
[71] G.R. Steinberg, D. Carling, AMP-activated protein kinase: the current landscape for drug development, Nat. Rev. Drug Discov. 18 (7) (2019) 527–551.
[72] X.F. Li, S.Y. Li, C.M. Dai, et al., PP2A inhibition by LB-100 protects retinal pigment epithelium cells from UV radiation via activation of AMPK signaling, Biochem. Biophys. Res. Commun. 506 (1) (2018) 73–80.
[73] S. Li, U. Gaur, C.M. Chong, et al., Berberine protects human retinal pigment epithelial Cells from hydrogen peroxide-induced oxidative damage through activation of AMPK, Int. J. Mol. Sci. 19 (6) (2018) 1736.
[74] C.L. Chen, Y.H. Chen, C.M. Liang, et al., Glucosamine-induced autophagy through AMPK(-)mTOR pathway attenuates lipofuscin-like autofluorescence in human retinal pigment epithelial cells in vitro, Int. J. Mol. Sci. 19 (5) (2018) 1416.
[75] K.R. Li, Z.Q. Zhang, J. Yao, et al., Ginsenoside Rg-1 protects retinal pigment epithelium (RPE) cells from cobalt chloride ($CoCl_2$) and hypoxia assaults, PLoS One 8 (12) (2013), e84171.
[76] A.L. Dafre, A.E. Schmitz, P. Maher, Methylglyoxal-induced AMPK activation leads to autophagic degradation of thioredoxin 1 and glyoxalase 2 in HT22 nerve cells, Free Radic. Biol. Med. 108 (2017) 270–279.
[77] S.W. Kang, G. Haydar, C. Taniane, et al., AMPK activation prevents and reverses drug-induced mitochondrial and hepatocyte injury by promoting mitochondrial fusion and function, PLoS One 11 (10) (2016), e0165638.
[78] H. Meng, Q.Y. Wang, N. Li, et al., Danqi tablet regulates energy metabolism in ischemic heart rat model through AMPK/SIRT1-PGC-1alpha pathway, Chin. J. Integr. Med. 27 (8) (2021) 597–603.
[79] H. Nanjaiah, B. Vallikannan, Lutein upregulates the PGC-1alpha, NRF1, and TFAM expression by AMPK activation and downregulates ROS to maintain mtDNA integrity and mitochondrial biogenesis in hyperglycemic ARPE-19 cells and rat retina, Biotechnol. Appl. Biochem. 66 (6) (2019) 999–1009.
[80] A.S. Ibrahim, K. Hussein, F. Wang, et al., Bone morphogenetic protein (BMP)4 but not BMP2 disrupts the barrier integrity of retinal pigment epithelia and induces their migration: a potential role in neovascular age-related macular degeneration, J. Clin. Med. 9 (7) (2020) 2293.
[81] M. Zhou, J.S. Geathers, S.L. Grillo, et al., Role of epithelial-mesenchymal transition in retinal pigment epithelium dysfunction, Front. Cell Dev. Biol. 8 (2020) 501.
[82] M. Saeed, M.A. Kausar, R. Singh, et al., The role of glyoxalase in glycation and carbonyl stress induced metabolic disorders, Curr. Protein Pept. Sci. 21 (9) (2020) 846–859.
[83] A.K. Berner, O. Brouwers, R. Pringle, et al., Protection against methylglyoxal-derived AGEs by regulation of glyoxalase 1 prevents retinal neuroglial and vasodegenerative pathology, Diabetologia 55 (3) (2012) 845–854.
[84] R. Sachdeva, A. Schlotterer, D. Schumacher, et al., TRPC proteins contribute to development of diabetic retinopathy and regulate glyoxalase 1 activity and methylglyoxal accumulation, Mol. Metabol. 9 (2018) 156–167.
[85] D.E. Maessen, C.D. Stehouwer, C.G. Schalkwijk, The role of methylglyoxal and the glyoxalase system in diabetes and other age-related diseases, Clin. Sci. (Lond.) 128 (12) (2015) 839–861.
[86] S. Rowan, E. Bejarano, A. Taylor, Mechanistic targeting of advanced glycation end-products in age-related diseases, Biochim. Biophys. Acta, Mol. Basis Dis. 1864 (12) (2018) 3631–3643.
[87] N. Rabbani, M. Xue, M.O. Weickert, P.J. Thornalley, Reversal of insulin resistance in overweight and obese subjects by trans-resveratrol and hesperetin combination-link to dysglycemia, blood pressure, dyslipidemia, and low-grade inflammation, Nutrients 13 (7) (2021) 2374.
[88] N.M.J. Hanssen, J. Westerink, J. Scheijen, et al., Higher plasma methylglyoxal levels are associated with incident cardiovascular disease and mortality in individuals with type 2 diabetes, Diabetes Care 41 (8) (2018) 1689–1695.
[89] A.S. Peters, M. Wortmann, T.H. Fleming, et al., Effect of metformin treatment in patients with type 2 diabetes with respect to glyoxalase 1 activity in atherosclerotic lesions, Vasa 48 (2) (2019) 186–192.

[90] M. Xue, N. Rabbani, H. Momiji, et al., Transcriptional control of glyoxalase 1 by Nrf2 provides a stress-responsive defence against dicarbonyl glycation, Biochem. J. 443 (1) (2012) 213–222.
[91] M. Matzinger, K. Fischhuber, D. Poloske, et al., AMPK leads to phosphorylation of the transcription factor Nrf2, tuning transactivation of selected target genes, Redox Biol. 29 (2020), 101393.
[92] N. Rabbani, P.J. Thornalley, Glyoxalase 1 modulation in obesity and diabetes, Antioxidants Redox Signal. 30 (3) (2019) 354–374.
[93] J.H. Lee, L. Subedi, S.Y. Kim, Effect of cysteine on methylglyoxal-induced renal damage in mesangial cells, Cells 9 (1) (2020) 234.